NASA / TM-2001-211028

Compact Ozone Differential Absorption Lidar (DIAL) Transmitter Using Solid-State Dye Polymers

Alton L. Jones, Jr.
Old Dominion University, Norfolk, Virginia

Russell J. DeYoung
Langley Research Center, Hampton, Virginia

Hani Elsayid-Ele
Old Dominion University, Norfolk, Virginia

July 2001

The NASA STI Program Office . . . in Profile

Since its founding, NASA has been dedicated to the advancement of aeronautics and space science. The NASA Scientific and Technical Information (STI) Program Office plays a key part in helping NASA maintain this important role.

The NASA STI Program Office is operated by Langley Research Center, the lead center for NASA's scientific and technical information. The NASA STI Program Office provides access to the NASA STI Database, the largest collection of aeronautical and space science STI in the world. The Program Office is also NASA's institutional mechanism for disseminating the results of its research and development activities. These results are published by NASA in the NASA STI Report Series, which includes the following report types:

- TECHNICAL PUBLICATION. Reports of completed research or a major significant phase of research that present the results of NASA programs and include extensive data or theoretical analysis. Includes compilations of significant scientific and technical data and information deemed to be of continuing reference value. NASA counterpart of peer-reviewed formal professional papers, but having less stringent limitations on manuscript length and extent of graphic presentations.

- TECHNICAL MEMORANDUM. Scientific and technical findings that are preliminary or of specialized interest, e.g., quick release reports, working papers, and bibliographies that contain minimal annotation. Does not contain extensive analysis.

- CONTRACTOR REPORT. Scientific and technical findings by NASA-sponsored contractors and grantees.

- CONFERENCE PUBLICATION. Collected papers from scientific and technical conferences, symposia, seminars, or other meetings sponsored or co-sponsored by NASA.

- SPECIAL PUBLICATION. Scientific, technical, or historical information from NASA programs, projects, and missions, often concerned with subjects having substantial public interest.

- TECHNICAL TRANSLATION. English-language translations of foreign scientific and technical material pertinent to NASA's mission.

Specialized services that complement the STI Program Office's diverse offerings include creating custom thesauri, building customized databases, organizing and publishing research results . . . even providing videos.

For more information about the NASA STI Program Office, see the following:

- Access the NASA STI Program Home Page at *http://www.sti.nasa.gov*

- Email your question via the Internet to help@sti.nasa.gov

- Fax your question to the NASA STI Help Desk at (301) 621-0134

- Telephone the NASA STI Help Desk at (301) 621-0390

- Write to:
  NASA STI Help Desk
  NASA Center for AeroSpace Information
  7121 Standard Drive
  Hanover, MD 21076-1320

NASA/TM-2001-211028

Compact Ozone Differential Absorption Lidar (DIAL) Transmitter Using Solid-State Dye Polymers

Alton L. Jones, Jr.
Old Dominion University, Norfolk, Virginia

Russell J. DeYoung
Langley Research Center, Hampton, Virginia

Hani Elsayid-Ele
Old Dominion University, Norfolk, Virginia

National Aeronautics and
Space Administration

Langley Research Center
Hampton, Virginia 23681-2199

July 2001

Acknowledgments

I would like to thank all the personnel of the Atmospheric Science Division at the Langley Research Center who helped me with my questions about the research for this report. I would also like to thank Robert Hermes who provided the first samples of the solid-state dye polymer used in this research effort and all the people who helped in one way or another in the work done for this report.

Available from:

NASA Center for AeroSpace Information (CASI)
7121 Standard Drive
Hanover, MD 21076-1320
(301) 621-0390

National Technical Information Service (NTIS)
5285 Port Royal Road
Springfield, VA 22161-2171
(703) 605-6000

Contents

List of Tables

List of Figures

Summary

The measurement of atmospheric ozone is important because in the troposphere it is a pollutant that is toxic to living systems, but in the stratosphere ozone protects life by shielding us from the harmful ultraviolet-B (UV-B) radiation of the Sun. From aircraft, laser remote sensing using differential absorption lidar (DIAL) has become a very important technique for measuring atmospheric ozone at different altitudes and locations. Current aircraft-based DIAL systems use pulsed Nd:YAG pumped liquid dye lasers, which are then frequency doubled into the UV region, to probe both the stratosphere and troposphere for ozone.

This report describes a new potential DIAL laser transmitter using solid-state dye laser materials to make a simpler, more compact, lower mass laser system. Two solid-state dye laser materials were tested to evaluate their performance in a laser oscillator cavity end pumped by a pulsed Nd:YAG laser at 532 nm. Both dye laser materials are made from a solid-state polymer host polymethyl-methacrylate (PMMA) where one of the materials was injected with a pyrromethene laser dye, PM 580, and the other with PM 597. A narrowband laser oscillator cavity was constructed to produce visible wavelengths of 578 and 600 nm. The visible wavelengths produced by the PM 597 dye laser material were frequency doubled into the UV region (289 or 300 nm) by using a beta barium borate (BBO) crystal. The oscillator cavity produced a maximum energy of 11 mJ at a wavelength of 578 nm when pumped by the Nd:YAG laser at an energy of 100 mJ (532 nm) and pulse repetition rate of 10 Hz. A maximum output energy of 378 μJ was achieved in the UV region at a wavelength of 289 nm but lasted only 2000 laser shots at a repetition rate of 10 Hz. A computer model was used to predict the conversion efficiency of the BBO nonlinear crystal for comparison between theory and experimental results. The results are promising and show that a solid-state dye laser based ozone DIAL system is possible with improvements in the design of the laser transmitter.

1. Introduction

1.1. Importance of Ozone in Atmosphere

The distribution of ozone in the Earth's atmosphere has been studied for many decades (refs. 1 and 2). Ozone is a rare molecular species that averages about 3 molecules for every 10 million molecules of air. A large majority of ozone is distributed within two regions of the Earth's atmosphere called the troposphere and the stratosphere. Ninety percent of ozone in the atmosphere lies in an area approximately 10 to 50 km above the Earth's surface in a region called the stratosphere. The remaining ozone lies in a region from sea level up to approximately 10 km called the troposphere. In the troposphere, increases in ozone are of concern because of its direct contact with life forms. High levels are toxic to living systems and can severely damage the tissues of plants and animals (ref. 3). A large amount of surface-level ozone contributes to smog in many cities around the world and is increasingly being observed in rural areas as well (ref. 4). On the other hand, ozone in the stratosphere has the beneficial effect of blocking the harmful ultraviolet radiation of the Sun. Human-created compounds such as chlorofluorocarbons (CFCs) and related chemicals have contributed to the destruction of ozone in this region of the atmosphere (ref. 5). This depletion results in an increase in the level of ultraviolet-B (UV-B) radiation reaching the Earth's surface, which has a negative effect on human and plant life (ref. 6). In order to observe the changes of ozone in the atmosphere, it is necessary to monitor its concentrations at different altitudes and locations around the Earth.

1.2. Methods of Ozone Measurement

Several different methods are available to measure atmospheric ozone concentrations. These methods include measurement from weather balloons, from aircraft, and from space. Weather balloons allow in situ sampling of ozone but are limited to measure within the vicinity of the instrument (ref. 7). They provide a high-resolution profile of ozone concentration, but because of the large spatial variability of ozone in the atmosphere, weather balloons cannot be relied on to give a regional profile of ozone (ref. 7). Measurement of ozone from space is accomplished by using science instruments on satellites such as Nimbus-7 and Meteor-3 (ref. 8). The Total Ozone Mapping Spectrometer (TOMS) is an instrument used to provide global measurements of total column ozone, measured in Dobson units, on a daily basis (ref. 8). Figure 1 shows an example of a typical measurement made by the TOMS instrument. Instruments such as TOMS that take measurements of ozone from space are limited by their lack of vertical resolution; thus, they have difficulty measuring ozone concentrations in the lower atmosphere. Their advantage lies in the ability to create a global profile of ozone.

Laser remote sensing from aircraft with lidar (light detection and ranging) has become a very important technique for measuring ozone in the atmosphere. It has been used to measure the concentration of air pollution in urban areas, the chemical emission around industrial plants, and atmospheric trace chemicals in the stratosphere (ref. 9). Lidar uses lasers to probe the atmosphere and analyze the backscattered laser energy to yield information on molecular and aerosol densities. Aircraft-based lidar systems have the advantage of balloon measurements because they produce good vertical profiles and also have the advantage of space measurements in that large areas of the atmosphere can be profiled.

A basic lidar system consists of a pulsed laser source, a telescope receiver, a light detector, and a computer for data analysis. A laser pulse is fired into the atmosphere and collides with the molecules and aerosols, which scatter some of the light back to the receiver. The receiver collects this backscattered radiation, and the light detector transforms the radiation into an electrical pulse. This pulse is then sent to a computer for analysis. Early lidar measurements were made by Fiocco and

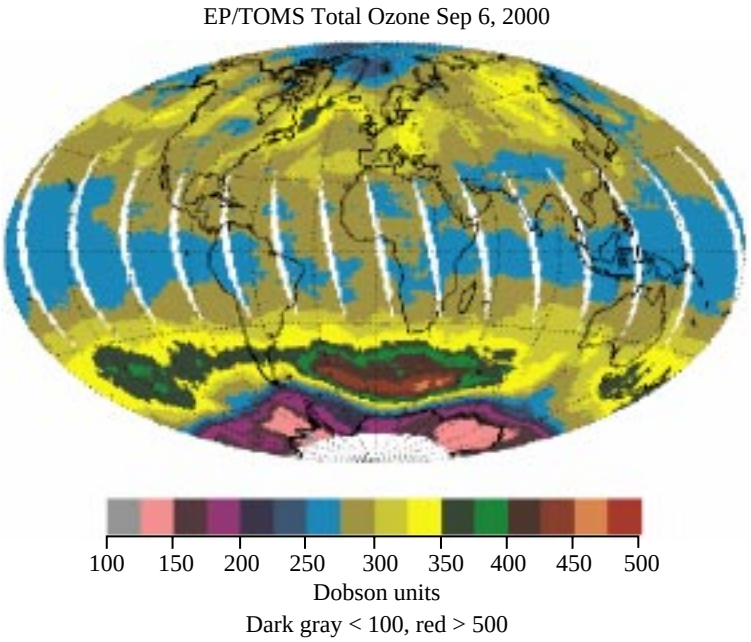

Figure 1. Complete global image of measurement of ozone in atmosphere from TOMS (ref. 8).

Smullin who bounced a pulsed laser beam off the Moon in 1962 (ref. 10). In 1964, Schotland used a temperature-tuned ruby laser to detect water vapor in the atmosphere (ref. 11).

1.3. Differential Absorption Lidar (DIAL) Technique

The Langley Research Center has an active aircraft-based research program that presently uses Nd:YAG pumped liquid dye lasers that are doubled into the UV region to probe both the stratosphere and troposphere for ozone by using the DIAL (differential absorption lidar) technique (ref. 7). The DIAL technique is a specialized lidar technique that can measure the absolute concentration of molecules in the atmosphere as a function of altitude. The airborne DIAL laser system has the flexibility to determine the spatial distribution of gases such as ozone, water vapor, sulfur dioxide, and nitrogen dioxide at multiple laser wavelengths (ref. 12). This DIAL laser system shown in figure 2 is comprised of two frequency doubled Nd:YAG lasers that pump two frequency doubled tunable dye lasers which transmit two laser beams separated in time at distinct wavelengths called the “on-line” beam and the “off-line” beam. One dye laser is tuned to a higher absorption spectrum of ozone at 289 nm (doubled 578 nm) for the DIAL on-line laser beam, whereas the other dye laser is tuned to 300 nm (doubled 600 nm) for the DIAL off-line wavelength (ref. 7). Each laser beam is transmitted in the zenith and nadir directions for the investigation of ozone distributions in the troposphere and lower stratosphere. The receiver system consists of two telescopes that are used to collect data above and below the aircraft. Photomultiplier tubes (PMT) are used to detect the backscattered light from the laser pulses propagating in the atmosphere. Digitizers are then used to digitize the analog signals created by the PMT to be stored as raw data on a magnetic tape. Once the data are saved, they may be analyzed by the computer to display the ozone concentration as a function of altitude.

Airborne lidar measurements have a great advantage in their flexibility. This flexibility makes it possible to fly frequent missions over areas of interest and allows researchers to monitor the changes of ozone concentrations during the seasons of the year at many different locations. In the future, flying autonomous, lightweight, compact ozone DIAL instruments on unpiloted atmospheric vehicles (UAV)

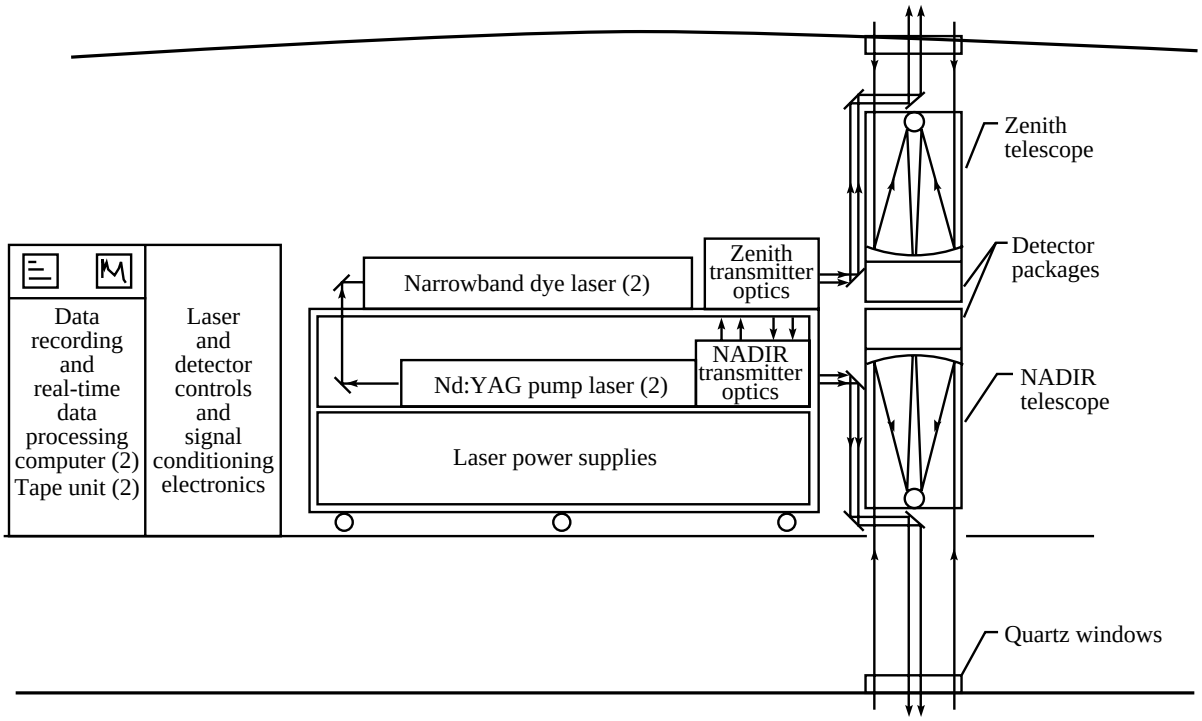

Figure 2. Block diagram of airborne DIAL system used by Langley Research Center (ref. 7).

will be desirable. This type of vehicle could fly at high altitudes for extended periods of time collecting scientific data without risk to the pilot. The cost for such missions may be significantly reduced in comparison with the present large aircraft-based missions (ref. 13). Unfortunately, the current ozone DIAL system is too massive to fly on this type of aircraft. This research effort may be one step toward the ability to fly DIAL systems on UAV aircraft.

One requirement of remote sensing is the availability of lasers with sufficient tunable laser energy to provide adequate lidar signals. The NASA DIAL laser system uses liquid dyes to fulfill this requirement. Dye chemicals are dissolved in a solvent and pumped continuously through a cell where the 532 nm doubled Nd:YAG laser pumps the liquid dye. The laser beam excites the molecules in the dye solution and emits a laser beam at a visible wavelength. This output is then frequency doubled by angle-tuned temperature-stabilized potassium and dihydrogen phosphate (KDP) crystals into the UV region. With the addition of a diffraction grating, this process allows the dye lasers to be tuned to the wavelength of interest. The output power of the dye laser beam decreases over time because of the damaging effect the pump laser beam has on the dye solution. The use of liquid dye solutions could impose harmful effects on the environment if not properly disposed. To eliminate this problem and also to produce a more compact laser system, researchers have explored the use of solid-state materials or plastics that are injected with dye chemicals allowing the laser to operate at visible wavelengths. Significant advancements have been made in the production of laser dye molecules and the formation of solid-state polymer materials. The use of these materials results in a more compact laser device with a fire-safe, nontoxic dye. They also eliminate inhomogeneties connected with liquid flow fluctuations and solvent vaporization associated with liquid dye pumps (ref. 14).

1.4. Characteristics of Dye Lasers

Dye lasers are the most versatile class of lasers because of the unlimited variety of dye molecules that can be used as an active medium (ref. 15). Solid-state dye lasers provide an alternative to the more

commonly used liquid dyes in tuning lasers to specific wavelengths. They eliminate the need for electric-powered fluid pumps making the overall system more compact and reducing the risk of spillage or leakage of the gain medium into the environment. Significant advancements have been made in the production of laser dye molecules and the formation of solid-state polymer hosts (ref. 16). The first attempt at an active solid-state dye laser operation was made in 1967–1968 when lasing was achieved in a rhodamine dye doped in polymethyl-methacrylate (PMMA) (ref. 17). The results from this experiment yielded low efficiency and low photostability. In recent years, new efficient dyes have been obtained along with new ways of dye input into the host matrix to produce higher efficiencies (ref. 16). The pyrromethene family of dyes has demonstrated very high efficiencies under laser pumping over a range of wavelengths (ref. 18). In solution, pyrromethene-BF_2 (PM) complexes offer strong absorption (λ_{max} = 490–580 nm) and laser activity (λ_{laser} = 540–670 nm) (ref. 19). These pyrromethene-based dye lasers have outperformed the rhodamine and coumarin dyes in the same wavelength ranges under flashlamp and laser pumping (ref. 20). PMMA has the greatest potential for a host matrix because its structure is close to the structure of dyes, and it has a high optical homogeneity (ref. 14). Modifications of PMMA, better known as modified polymethyl-methacrylate (MPMMA), have been produced through the use of copolymers and additives to increase the damage resistance and the overall efficiency of the solid-state dye laser. Pyrromethene-BF_2 (PM) complexes doped in MPMMA show excellent laser efficiency and damage resistance when excited at a wavelength of 532 nm (ref. 16).

Laser emission from solid-state dye materials may be obtained by using a simple oscillator cavity design consisting of two mirrors and the dye material as the gain medium. The dye molecules inside the dye host material are excited to higher energy levels to create a population inversion by end pumping the oscillator cavity with a frequency doubled Nd:YAG laser at 532 nm. Once the molecules are in the excited state, they quickly relax to a lower state emitting photons that are shifted to longer wavelengths in comparison with the pump wavelength. The spectral region of the laser output is dependent upon the type of dye used for the gain medium.

Surface damage of the host material and dye darkening or bleaching inside the host material are the two main damage mechanisms caused by the high intensity of the pump laser (ref. 16). This bleaching effect is more acute for solid-state systems than for those that are solvent based because flowing liquid systems allow for continual refreshing of the gain medium. The dye eventually degrades, and the pumped area needs to be either translated or rotated to a fresh spot. Modified solid-state polymers such as MPMMA have now been developed to resist laser radiation as high as those of most laser damage-resistant inorganic glasses and crystals (ref. 21). These polymers provide control of the characteristics of high-power laser radiation that is needed for efficient doubling into the UV region. The MPMMA material is a suitable choice for use in an ozone DIAL laser system because of the need for long-term dye stability and high efficiency during operation on science missions.

1.5. Research Goal

The goal of this investigation is to design, construct, and test a compact dye laser transmitter using a solid-state polymer laser material. This investigation is presented in detail in reference 22. The material is tested in a series of experiments to define the laser oscillator parameters necessary for the most efficient laser action. Optical tuning elements are placed inside the oscillator cavity to provide a range of visible wavelengths necessary for frequency doubling into the UV region to produce wavelengths of 289 and 300 nm. The oscillator cavity is optimized to produce a laser output with high energy, narrow line width, and small beam divergence necessary for efficient frequency doubling using a nonlinear crystal. The measured conversion efficiency is compared with the modeling results of the nonlinear crystal characteristics.

2. Theory

This section covers the theory behind and the derivation of the DIAL equation for measuring atmospheric ozone and also the theory of second harmonic generation used to convert the dye laser output into the UV region. First this section begins with the derivation of the DIAL equation from the lidar equation. The theory of second harmonic generation is then covered. Finally, theoretical calculations of second harmonic conversion efficiencies are made to set goals for expected experimental results.

2.1. Lidar Equation

Lidar is similar to radar but uses optical wavelengths. A basic lidar system is composed of a transmitter and receiver as shown in figure 3 (ref. 23). A short laser pulse at a specific wavelength is directed into the atmosphere through the use of a laser transmitter. A portion of the energy contained in the laser pulse is scattered from the atmospheric constituents such as molecules, aerosols, clouds, or dust. This reflected radiation is detected by a receiver system that is used to determine the relative concentration of the interacting species over the targeted region of the atmosphere. In addition to the relative concentration, the range of the interacting species can be determined from the temporal delay of the backscattered radiation. Lidar has been used to measure air pollution in urban areas and chemical emissions around industrial plants (ref. 9).

The lidar equation is used to predict the telescope power received from the back-scattered atmospheric signal and is given as

$$P_r = \frac{P_t \rho A K \exp(-2\alpha R)}{R^2} \tag{1}$$

where

P_r laser power scattered back to receiver telescope

P_t power transmitted by laser

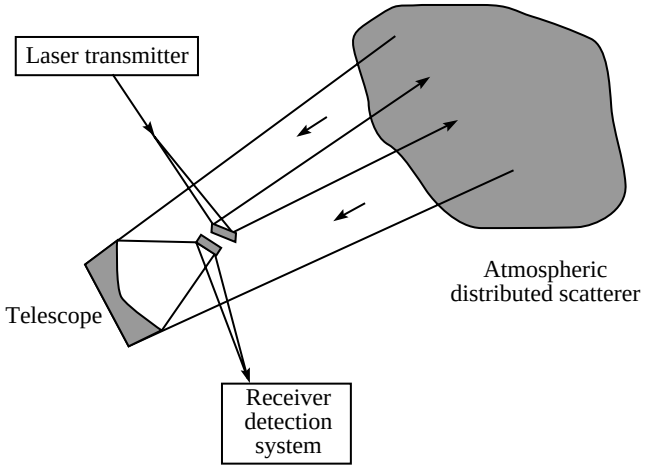

Figure 3. Schematic diagram of typical lidar system (ref. 23).

R range or distance from receiver to target

ρ effective reflectivity of targeted species

A area of telescope

K optical efficiency of receiver system

$\exp(-2\alpha R)$ two-way atmospheric attenuation of laser beam (ref. 9)

The scattering process reduces the intensity of the laser beam, which contributes to extinction. Both processes cause an attenuation of the laser beam due to Beer's law

$$I = I_o \exp(-\alpha R) \tag{2}$$

where

I intensity of laser beam after transmission over distance R

α atmospheric extinction coefficient

I_o original intensity of laser beam (ref. 9)

The atmospheric extinction coefficient may be expressed as a sum of terms as follows:

$$\alpha = \alpha_{\text{Ray}} + \alpha_{\text{Mie}} + \alpha_{\text{Raman}} + \alpha_{\text{abs}} \tag{3}$$

where α_{Ray}, α_{Mie}, and α_{Raman} are the extinction coefficients related to Rayleigh, Mie, and Raman scattering, respectively, and α_{abs} is the molecular absorption coefficient (ref. 24). Rayleigh scattering is a form of light scattering from particles in the atmosphere, such as molecules or fine dust that are much smaller than the optical wavelength of the laser. Mie scattering comes from small particles or aerosols that have a size comparable with or greater than the wavelength of radiation. The Rayleigh and Mie processes are a form of elastic scattering in which the scattered laser radiation is the same wavelength as the incident laser wavelength. Raman scattering is an inelastic interaction of the laser beam with the atmosphere involving excitation of the energy levels of a molecule resulting in a reradiation at a different wavelength. Absorption may be observed as the attenuation of the incident laser beam when the laser frequency matches the absorption band of a given molecule leading to the excitation of the molecule followed by a radiative or nonradiative decay (ref. 9).

The elastic scattering form of the basic lidar equation includes the optical parameters of the receiver system (ref. 23) and is given as

$$P(\lambda,R) = C(\lambda,R)\, P_L(\lambda)\, \frac{A_r}{R^2}\, \Delta R\, T^2(\lambda,R)\, \beta(\lambda,R) \tag{4}$$

where

$P(\lambda,R)$ received power at specific wavelength

R range from receiver to targeted species

$C(\lambda,R)$ system function determined by optical parameters of receiver optics, quantum efficiency of detection system, and overlap of transmitted laser beam with field of view of telescope

$P_L(\lambda)$ average laser power emitted into atmosphere

A_r/R^2 acceptance solid angle of receiving optics

A_r collecting area of telescope

$\beta(\lambda,R)$ back scattering coefficient

R range to target

ΔR range resolution of lidar signal given by $\dfrac{c(\tau_L + \tau_d)}{2}$

τ_L, τ_d laser pulse duration and data acquisition resolution time, respectively

c speed of light

$T^2(\lambda,R)$ two-way transmission factor of laser beam to range R at wavelength λ, approximated by the Lambert-Beer law (ref. 23) and given by

$$T^2(\lambda,R) = \exp\left[-2\int_0^R \alpha(\lambda,r)\, dr\right] \tag{5}$$

To detect a species from a long distance, a laser beam must not be significantly attenuated by the atmosphere. The output wavelength of the laser must lie in a spectral transmission window of the atmosphere. These windows are shown as clear areas in figure 4, which shows areas of high transmission in wavelength regions needed for lidar measurements. The absorption regions are due primarily to oxygen, carbon dioxide, and water vapor (ref. 9). The most effective transparent spectral ranges of the atmosphere are located in the visible range (0.4 to 0.7 μm) and the infrared range (0.7 to 1.5 μm, 3 to 5 μm, and 9 to 13 μm). The laser beam is not significantly attenuated within these spectral regions except by clouds and aerosols and allows remote sensing of the atmosphere over long distances.

The scattering form of the lidar equation given in equation (4) assumes that only single scattering events occur. Laser photons that are emitted from a laser source are scattered only once before reaching the detector. When the optical depth of the probed medium or atmosphere exceeds approximately 0.3, multiple scattering becomes significant because possibly two or more scattering events by molecules or

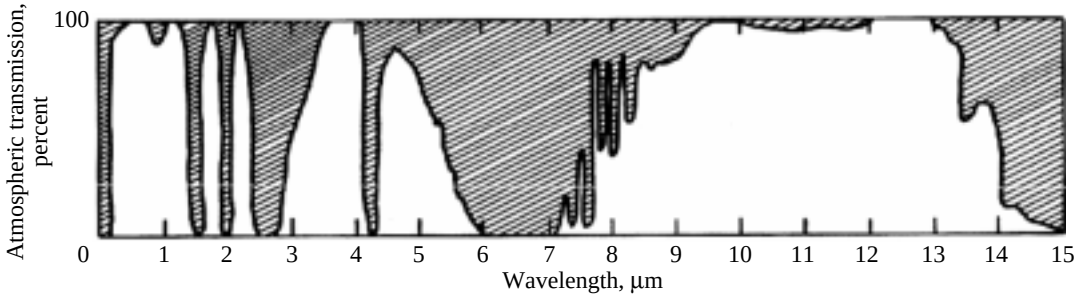

Figure 4. Absorption regions and transmission windows in atmosphere over 0.3-km path near sea level from 0.2 to 15 μm (ref. 9).

particles occur before reaching the detector. This scattering may occur in heavily polluted environments. The analysis of a multiple-scattered lidar signal is much more difficult than for single scattering.

The use of lidar and the lidar equation only gives a relative indication of the number of scatters in the atmosphere. It does not give any information about the scattering species or its concentration in a particular region of the atmosphere. For this information, a special type of lidar called differential absorption lidar (DIAL) is used to measure the concentration of atmospheric scatters of a particular type.

2.2. DIAL Equation

The DIAL technique is used for the remote measurement of ozone profiles in the upper and lower atmosphere. This technique uses two laser wavelengths to measure the difference in the absorption of the lidar signal between a wavelength that is absorbed by ozone molecules in the atmosphere called the on-line wavelength and a wavelength that is less absorbed called the off-line wavelength. The ground-based application of the DIAL technique permits frequent measurement of ozone profiles at a specific location. In this technique, the average gas concentration over some selected range interval is determined by analyzing the power of the lidar backscattered signals for laser wavelengths tuned "on" (λ_{on}) and "off" (λ_{off}) the specific absorption of ozone molecules. The basic concept of the DIAL technique is shown in figure 5. The on-line and off-line wavelengths transmitted by the DIAL laser system are 289 and 300 nm, respectively. The absorption cross section of ozone is shown in figure 6 with both the on- and off-line wavelengths. The DIAL equation is the ratio of the received powers from both the on- and off-line laser beams and is given by

$$\frac{P_{on}(\lambda_{on},R)}{P_{off}(\lambda_{off},R)} = \frac{\beta(\lambda_{on},r)\ \exp\left[-2\int_0^R \alpha(\lambda_{on},r)\ dr\right]}{\beta(\lambda_{off},r)\ \exp\left[-2\int_0^R \alpha(\lambda_{off},r)\ dr\right]} \tag{6}$$

This equation is obtained from equation (4), with the constant system function $C(\lambda,R)$ canceling out in the ratio leaving the backscatter and extinction terms (ref. 8). By taking the natural logarithm and the derivative with respect to R, the concentration of the target species N is approximately

$$N = \frac{1}{2\Delta\sigma}\left\{\underbrace{\frac{\partial}{\partial R}\ln\frac{P_{on}(R,\lambda_{on})}{P_{off}(R,\lambda_{off})}}_{A} - \underbrace{\frac{\partial}{\partial R}\ln\frac{\beta(R,\lambda_{on})}{\beta(R,\lambda_{off})}}_{B} + \underbrace{2[\alpha(R,\lambda_{on})-\alpha(R,\lambda_{off})]}_{C}\right\} \tag{7}$$

where $\Delta\sigma = \sigma(\lambda_{on}) - \sigma(\lambda_{off})$ is the differential absorption cross section of the measured target species. The retrieved concentration N expressed in this equation is simplified by taking into account only the A term while the B and C terms from backscattering and extinction, respectively, are neglected. If the difference in wavelength is small, the backscattering coefficients are assumed to be essentially the same and the B term reduces to zero given a homogeneous atmosphere (ref. 7). The C term, which is due to the wavelength dependence of the aerosol attenuation, will also approach zero as the wavelength

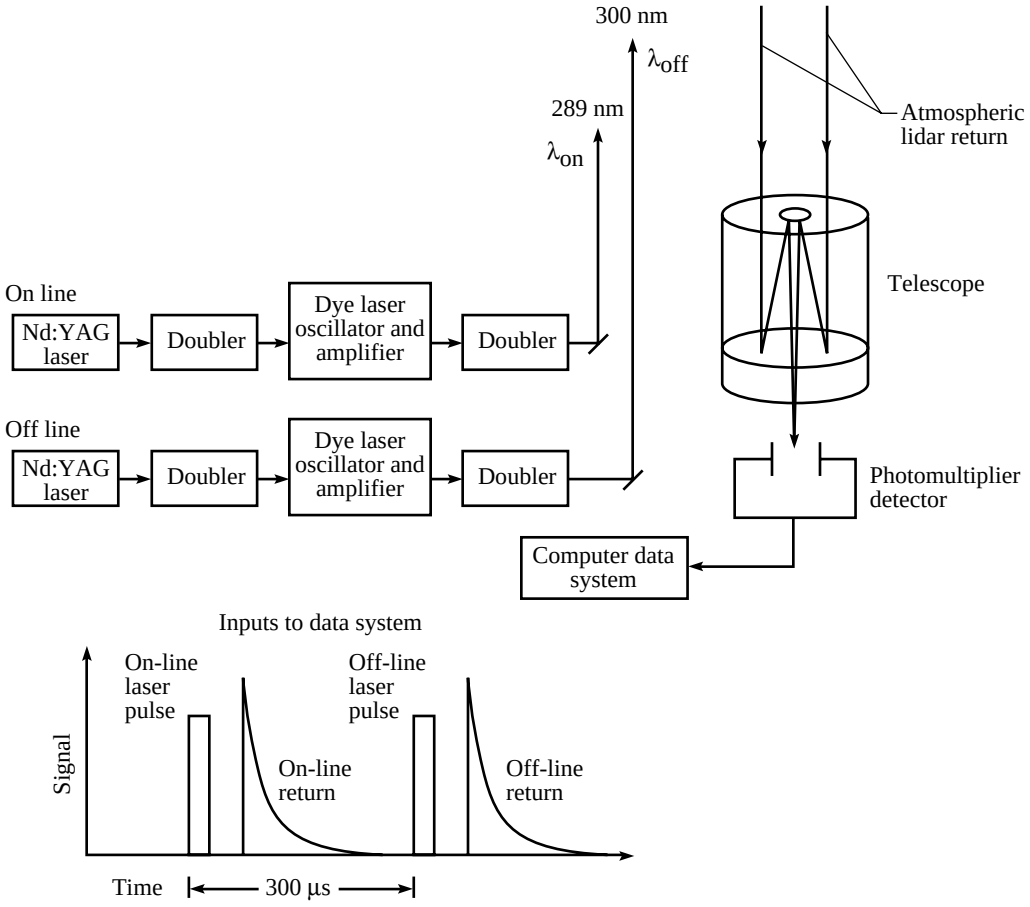

Figure 5. DIAL concept with on-line and off-line signals typically separated by 300 μs.

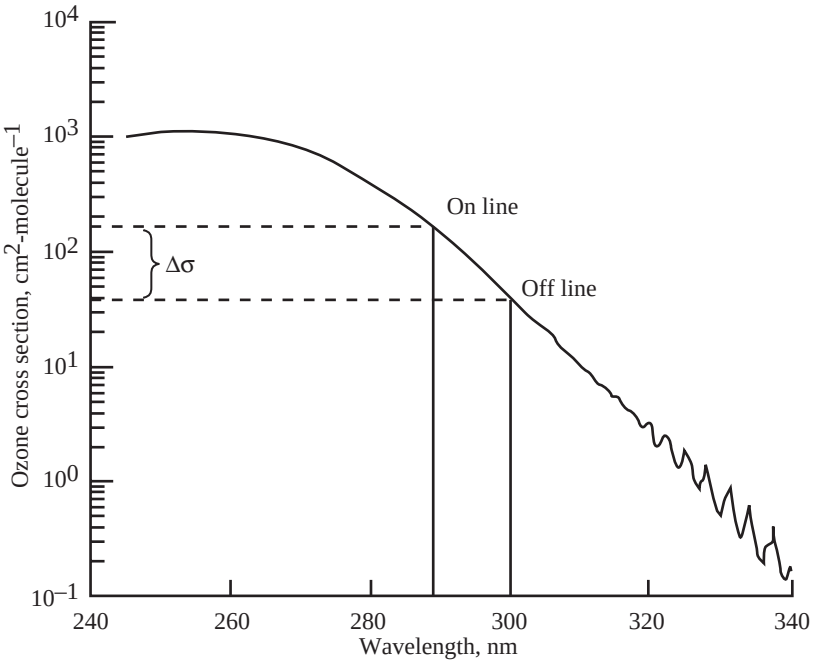

Figure 6. Absorption cross section of ozone with on- and off-line wavelengths at 289 and 300 nm, respectively.

separation of the on- and off-line wavelengths is reduced (ref. 7). The value of the ozone concentration N at a specific range can be determined by using a simplified version of equation (8) and is given as

$$N(R) = \frac{1}{2(R_2 - R_1)[\sigma(\lambda_{on}) - \sigma(\lambda_{off})]} \ln\left[\frac{P_{off}(R_2)P_{on}(R_1)}{P_{off}(R_1)P_{on}(R_2)}\right] \tag{8}$$

where $\sigma(\lambda_{on}) - (\sigma\lambda_{off})$ is the difference between the ozone absorption cross sections at the on- and off-line wavelengths, and $P_{on}(R)$ and $P_{off}(R)$ are the signal powers received from range R at the on- and off-line wavelengths (ref. 12). This form of the DIAL equation provides a means of calculating atmospheric ozone as a function of altitude. The ozone concentration is determined from the natural logarithm of the received powers for the on- and off-line return signals in a given range cell $(R_2 - R_1)$. The two laser wavelengths and the absorption cross section for ozone must be known when DIAL measurements are attempted.

2.3. Second Harmonic Conversion Theory

The dye lasers used in the airborne DIAL system produce wavelengths in the visible region. The on-line dye laser is tuned to 578 nm while the off-line dye laser is tuned to 600 nm. To extend the wavelength of this laser source into the UV region for ozone measurements, a frequency doubling crystal is used to generate the second harmonic of the fundamental dye laser wavelength. The first report of second harmonic generation through laser operation was in 1961 (ref. 25). A ruby laser with a wavelength of 694.3 nm was incident on a quartz crystal, which generated ultraviolet light at exactly one-half the wavelength of the incident laser radiation. Figure 7 shows a block diagram of the basic principle of second harmonic generation. Second harmonic generation may also be viewed as the exchange of photons between the various frequency components of the electric field. Figure 8 shows an illustration of this interaction where two photons of frequency f are destroyed and a photon of frequency $2f$ is simultaneously created in a single quantum-mechanical process (ref. 26). The solid line in figure 8 represents the atomic ground state, and the dashed lines represent virtual levels of a nonlinear crystal. The physical process of frequency doubling through second harmonic generation is due primarily to the dependence of the polarization on the electric field. When an electric field enters a material, it induces a polarization

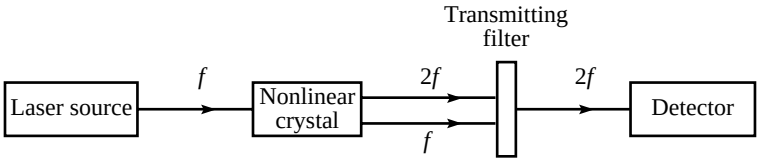

Figure 7. Block diagram of experimental arrangement for detection of second harmonic generation (ref. 25).

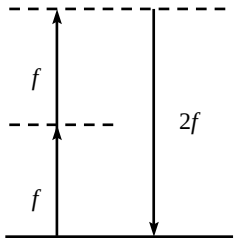

Figure 8. Energy level diagram describing second harmonic generation.

in the material. The propagation of a wave through the material produces changes in the distribution of electrical charges as the electrons and atoms react to the electromagnetic fields of the incident wave. The magnitude of the induced polarization per unit volume depends on the magnitude of the applied electric field (ref. 27). The relationship between polarization and electric field is given by

$$\bar{P}(t) = \chi^{(1)}\bar{E} + \chi^{(2)}\bar{E}^2 + \chi^{(3)}\bar{E}^3 + \ldots \tag{9}$$

where P is the induced polarization; χ is the first, second, and third-order susceptibility; and E in the magnitude of the electric field. The polarization may be assumed to vary linearly with the electric field, but with large values of E available from high power lasers this assumption is no longer valid. The first term in equation (9) is responsible for the ordinary linear optical effects. The following terms are responsible for what is normally called nonlinear optics. Because the higher orders of the susceptibility are small, the nonlinear optical effects start to show only when very high electrical fields are incident on a crystal. A laser beam whose electric field strength is represented as

$$\bar{E}(t) = E \exp(-i\omega t) + \text{c.c.} \tag{10}$$

where

c.c. = Complex conjugate

gives rise to the nonlinear polarization created inside the crystal for which the second-order susceptibility in equation (9) is nonzero. The induced polarization is

$$\bar{P}^{(2)}(t) = 2\chi^{(2)}EE^* + [\chi^{(2)}E^2 \exp(-2i\omega x) + \text{c.c.}] \tag{11}$$

where the first term consists of a contribution at zero frequency and the second term is a contribution at a frequency $2f$ (ref. 26). The latter contribution leads to the generation of radiation at the second harmonic frequency.

2.3.1. Parameters Affecting Second Harmonic Conversion Efficiency

The laser source in the second harmonic generation must have a high-power density, small beam divergence, and a narrow line width in order to achieve maximum second harmonic power (ref. 27). For conversion efficiency, the ratio of the power generated at the second harmonic frequency to that incident at the fundamental wave is given by (ref. 27):

$$\frac{P_{2\omega}}{P_{\omega}} = l^2 K \frac{P_{\omega}}{A} \frac{\sin^2(\Delta kl/2)}{(\Delta kl/2)^2} \tag{12}$$

where

$P_{2\omega}$ power generated at second harmonic frequency

P_{ω} incident laser power at fundamental wavelength

l length of nonlinear crystal

A area of fundamental beam

Δk phase mismatch between polarization wave and electromagnetic wave

K nonlinear coefficient which is constant for given wavelength and given nonlinear material

From equation (12), the second harmonic power generation is strongly dependent on the phase mismatch expressed by the $\sin^2 x/x^2$ function where $x = \Delta kl/2$ and is illustrated in figure 9. For $\Delta kl \neq 0$ the efficiency is reduced significantly. The phase matching bandwidth is defined as the points where the function is reduced to one half the maximum value. The distance over which this function goes to zero is defined as "the coherence length" (ref. 28), which is the distance from the entrance face of the crystal to the point at which the second harmonic power is at its maximum value. The second harmonic conversion efficiency is proportional to the square of the crystal length as indicated in equation (12). Without some method of phase matching the fundamental and second harmonic fields, the coherence length is usually very small, typically on the order of 10 μm (ref. 25).

2.3.2. Phase Matching

For efficient second harmonic generation, the phase velocities of the two waves must be identical so that the second harmonic generated at different points along the path of the nonlinear crystal add in phase (ref. 29). A polarization wave at the second harmonic frequency $2\omega_1$ is produced inside the crystal, which has a phase velocity and wavelength determined by the index of refraction of the fundamental wave. A transfer of energy from this polarization wave to an electromagnetic wave at a frequency 2ω takes place, and the index of refraction for the doubled frequency determines the phase velocity and the wavelength of this electromagnetic wave (ref. 27). If the created electromagnetic wave has the same phase as the original wave, the created waves will interact constructively along the polarization, building up intensity at the second harmonic wavelength. On the other hand, if a difference in the phase exists, the wave will not be very intense, and the second harmonic waves interact both constructively and destructively. The difference in phase arises when the created wave propagates through the medium with a different speed from the original wave; this is true for most materials because the refractive index and speed of light are wavelength dependent. The phase matching conditions of wave vectors can be either collinear (scalar phase matching) or noncollinear (vector phase matching) (ref. 30). The phase

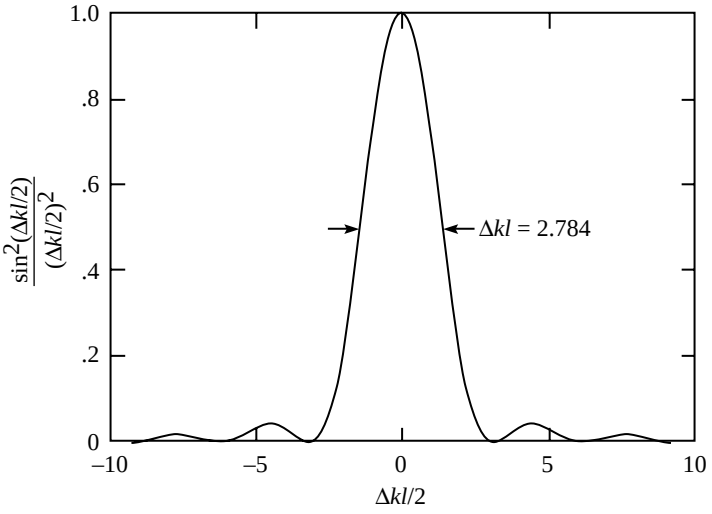

Figure 9. $\mathrm{Sin}^2 x/x^2$ function describing effects of phase mismatch in frequency conversion process.

mismatch between the polarization wave and the electromagnetic wave may be expressed as the difference in the wave number:

$$\Delta k = \frac{4\pi}{\lambda_1}(n_1 - n_2) \tag{13}$$

where λ_1 is the wavelength of the fundamental wave, n_1 is the index of refraction for the fundamental wave, and n_2 is the index of refraction of the doubled frequency. For efficient energy transfer to the second harmonic wavelength, Δk must equal zero which implies that $n_1 = n_2$. The phase matching condition $\Delta k = 0$ is difficult to achieve because of the differences in the indices of refraction for the fundamental and second harmonic wavelengths. The most common procedure for achieving phase matching is to make use of the birefringence displayed by many crystals (ref. 26). Birefringence is defined as the dependence of the refractive index on the direction of polarization (ref. 29). To produce a phase matching condition for two waves, mixing the ordinary and extraordinary waves in an anisotropic medium is possible (ref. 28). One of the waves, called the ordinary wave, sees a constant index of refraction n^o independent of its direction of propagation. The second wave, or the extraordinary wave, sees a refractive index $n^e(\theta)$ that is dependent on its direction of propagation. The angle θ describes the direction of propagation relative to one of the principal axes of the crystal (ref. 28). In a crystal where n^e is greater than n^o, phase matching may be achieved by finding the angle of propagation θ_{pm} to satisfy the equation

$$n^o_\omega = n^e_{2\omega}(\theta_{pm}) \tag{14}$$

which can also be written as

$$n^o_\omega - n^e_{2\omega}(\theta_{pm}) = 0 \tag{15}$$

where n^o and n^e are the ordinary and extraordinary refractive indices, respectively, and are graphically illustrated in figure 10 (ref. 28). Birefringent crystals have two types of angle phase matching (ref. 26). In second harmonic generation, type I phase matching is when either the ordinary or the extraordinary wave has the same polarization. In type II phase matching, the fundamental wavelength is polarized so that one of its orthogonal components is ordinary and the other is extraordinary.

The control of the refractive indices at each frequency is important in order to achieve the phase matching condition $\Delta k = 0$. In practice, angle tuning is a method used to achieve phase matching. Angle tuning involves the precise angular orientation of the crystal with respect to the propagation direction of the incident light. When the wave propagation is in a direction where the ordinary and extraordinary waves propagate with the same velocity, the refractive index for the extraordinary wave is given by (ref. 27):

$$n^e_{2\omega}(\theta_{pm}) = \frac{n^o_\omega n^e_{2\omega}}{\left[(n^o_\omega)^2 \sin^2 \theta_{pm} + (n^e_{2\omega})^2 \cos^2 \theta_{pm}\right]^{1/2}} \tag{16}$$

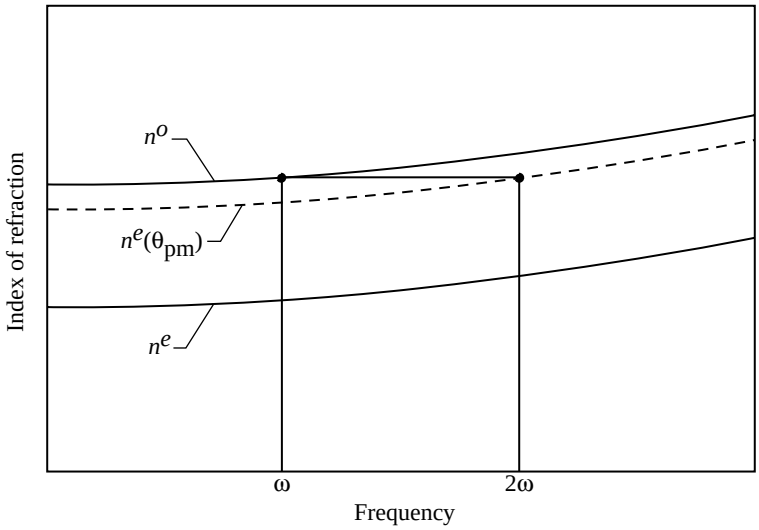

Figure 10. Illustration of method of matching refractive indices of fundamental and second harmonic waves in negative uniaxial crystal (ref. 28).

This expression can be approximated by (ref. 31):

$$n^e_{2\omega}(\theta_{pm}) = n^o_{2\omega} - (n^o_{2\omega} - n^e_{2\omega}) \sin^2 \theta_{pm} \tag{17}$$

An expansion of equation (15), taking into account small deviations from the phase matching direction θ_{pm}, yields (ref. 26)

$$n^o_{\omega} - n^e_{2\omega}(\theta_{pm}) = \frac{\partial\left[n^o_{\omega} - n^e_{2\omega}(\theta_{pm})\right]}{\partial\theta}(\theta - \theta_{pm}) \tag{18}$$

Substituting equation (17) into equation (18) results in (ref. 26)

$$n^o_{\omega} - n^e_{2\omega}(\theta) = \delta\theta(n^o_{2\omega} - n^e_{2\omega}) \sin 2\theta_{pm} \tag{19}$$

where $\delta\theta$ is interpreted as the beam divergence of the incident laser beam and is directly proportional to the ordinary and extraordinary indices of refraction. The incident laser beam must exhibit a small finite divergence to avoid defeating the phase matching condition.

In addition to the beam divergence, the spectral line width of the incident laser beam is also a critical factor in determining the efficiency of second harmonic generation. Expanding equation (15) to include small wavelength changes around the central wavelength λ_o at which phase matching occurs results in

$$n^o_{\omega} - n^e_{2\omega}(\theta_{pm}) = \left[\frac{\partial n^o_{\omega}}{\partial\lambda_{\omega}} - \frac{1}{2}\frac{\partial n^e_{2\omega}(\theta_{pm})}{\partial\lambda_{2\omega}}\right](\lambda - \lambda_o) \tag{20}$$

where $(\lambda - \lambda_o)$ is the spectral line width of the incident laser beam. Equation (20) shows that a large spectral spread of the line width would negatively affect the phase matching condition $n_{\omega}^{o} = n_{2\omega}^{e}(\theta_{pm})$ needed for efficient second harmonic generation.

2.4. Computer Model Used To Compute Conversion Efficiency

For the purpose of this experiment, theoretical calculations were made of the conversion efficiency by using a BBO nonlinear crystal to frequency double the solid-state visible dye laser. By using a computer model developed with the software program Mathsoft Mathcad, the second harmonic conversion efficiency was calculated from equation (12). The computer model calculates the conversion efficiency of the crystal in the following five separate steps:

1. The parameters for the dye laser beam at the input to the crystal must be defined and inserted into the model; the input parameters are defined as the energy of the incident dye laser beam (mJ), the spectral line width of the laser (pm), the divergence (mrad), the diameter of the laser beam at the full width at half maximum (mm), the pulse width of the laser (ns), and the length of the BBO crystal (mm)

2. The Δk term for the phase matching condition is calculated from the input parameters

3. The computer model divides the intensity of the input laser beam into 20 equally spaced sections where the amplitude inside each section is constant and joined together to represent a Gaussian intensity profile

4. The computer model calculates the conversion efficiency of each section by using differential equations (ref. 30) for a three-wave parametric interaction involving the second-order susceptibility defined in equation (9)

5. The conversion efficiency of each section is integrated to reflect the final conversion efficiency of the doubling crystal

Limitations of the computer model include (1) the assumption that the dye laser beam has a Gaussian intensity profile and (2) the computer model does not account for the walk-off angle of the doubling crystal. Errors in the calculation occur when defining wavelengths outside the transmission window of the doubling crystal and using negative values for the beam divergence. To simulate the expected experimental values for the solid-state dye laser beam with the computer model, two plots were made to predict the performance of the BBO doubling crystal. Figure 11 shows a plot of the efficiency as a function of the pump intensity for a 5-mm-long BBO doubling crystal with the incident laser beam having a line width of 300 pm for various divergences. As observed in figure 11, an improvement in the divergence as well as an increase in the pump intensity improves the efficiency of the BBO doubling crystal. For comparison, a second plot was made with the same input parameters but with a reduction in line width to 100 pm. As shown in figure 12, the efficiency of the crystal increases beyond 25 percent for high pump intensities at a line width of 100 pm.

To simulate near perfect conditions for the doubling crystal, a third plot shown in figure 13 was made for a dye laser beam at intensities near the damage threshold of the doubling crystal. The beam divergence was dropped to 0, and spectral line widths were kept between 1 and 4 pm. The highest possible or ideal performance from the BBO doubling crystal when using the computer model is 78 percent. The goal in this experiment is to produce a visible wavelength at 578 nm with the solid-state dye laser at

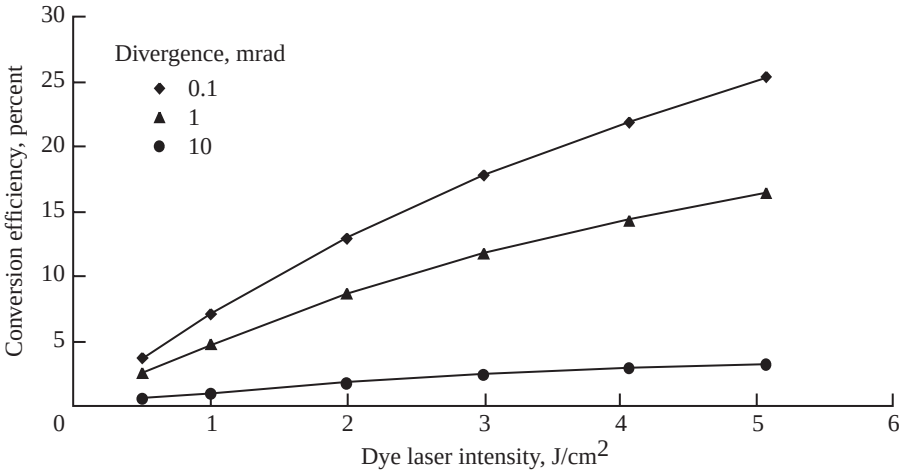

Figure 11. Efficiency of BBO doubling crystal at input line width of 300 pm for several different theoretical divergence measurements. Wavelength of dye laser, 578 nm.

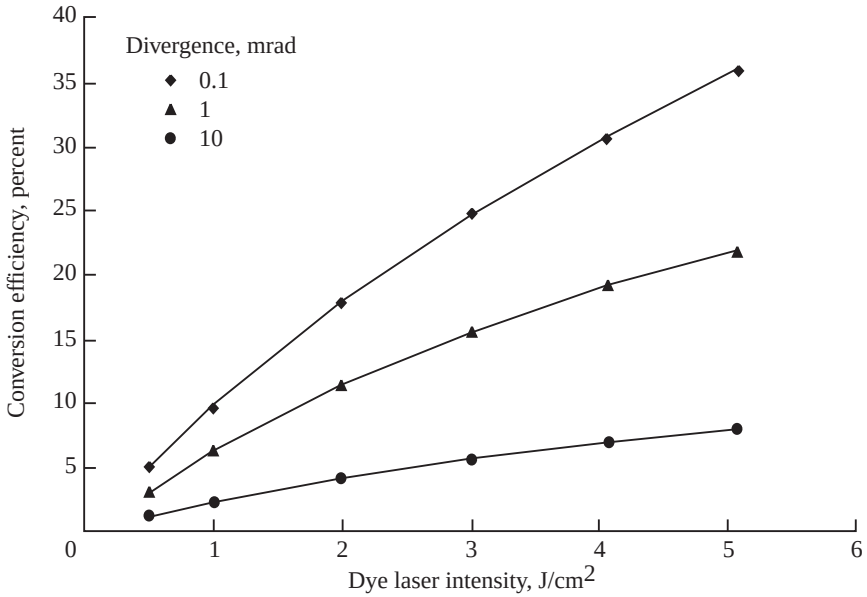

Figure 12. Efficiency of BBO doubling crystal at input line width of 100 pm for several different theoretical divergence measurements. Wavelength of dye laser, 578 nm.

a high-intensity level for a conversion efficiency of approximately 25 percent. The theoretical calculations are used to predict the second harmonic generation performance of the solid-state dye laser.

3. Solid-State Dye Laser Experimental Setup

This section describes the experimental setup for testing the characteristics of two different solid-state dye laser materials. The dye materials are polymer-host materials doped with pyrromethene laser dyes PM 580 and PM 597. A broadband and narrowband laser configuration is used to define important properties of the materials for possible use as an ozone DIAL laser transmitter.

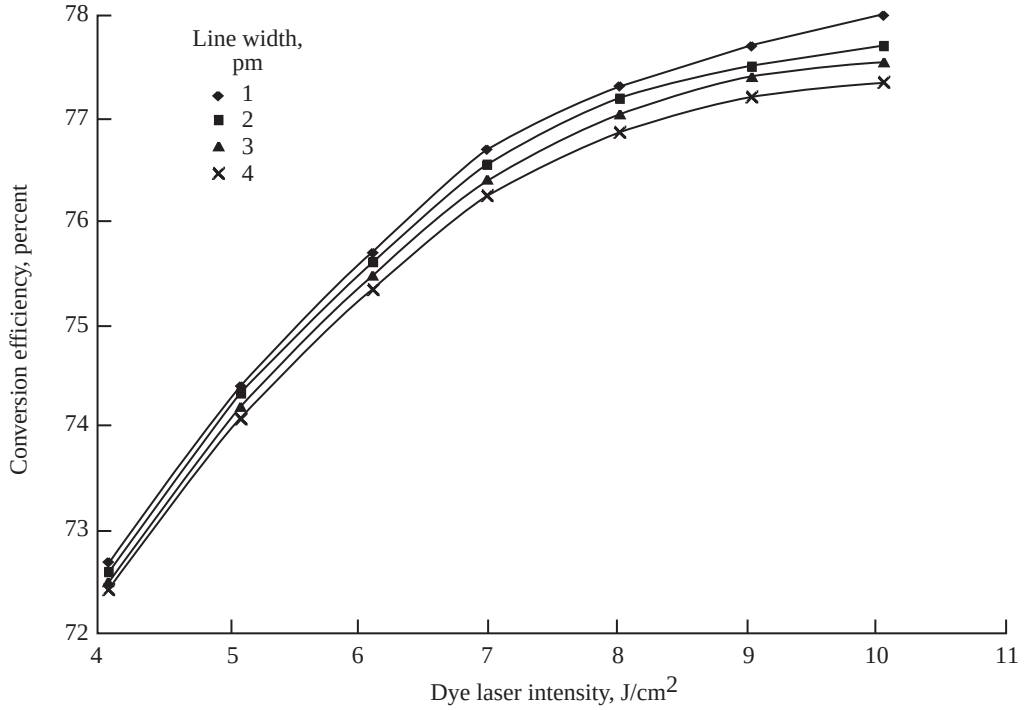

Figure 13. Efficiency of BBO doubling crystal at intensities near damage threshold of doubling crystal. Beam divergence held to 0 with spectral line widths from 1 to 4 pm.

3.1. Broadband Laser Cavity Configuration

A simple laser oscillator cavity consisting of two mirrors with the solid-state dye laser materials PM 580 and PM 597 as the gain medium was designed to measure the efficiency and lifetime of both laser materials. The oscillator cavity, shown in figure 14, was collinearly end pumped through the high reflector mirror by a frequency doubled Q-switched Nd:YAG laser at a wavelength of 532 nm. The Nd:YAG laser was flashlamp-pumped and produced a vertically polarized output beam 6 mm in diameter with a pulse width of 10 to 17 nsec (depending on the energy input to the flashlamps). The characteristics of this laser system are shown in table 1.

A dichroic mirror was used to separate the residual fundamental wavelength at 1064 nm from the second harmonic at 532 nm. The mirror was specially coated for a high reflectance at 532 nm at an angle of incidence of 45° and high transmission at 1064 nm for the same angle of incidence. A beam dump was placed behind the dichroic mirror to capture the residual 1064-nm laser beam. To control the 532-nm energy, a half-wave plate and cube polarizer were used to attenuate the power generated at this wavelength. The half-wave plate was used to rotate the polarization of the laser beam as it propagated through the cube polarizer. The polarizer was oriented in a direction for extinction of vertically polarized laser beams and transmission of horizontally polarized laser beams.

A dielectric-coated highly reflective plano mirror passed 98 percent of the 532-nm laser beam, and with a reflectivity greater than 97 percent between 560 and 620 nm, was used as the high reflector for the oscillator cavity. Figure 15 shows the transmission curve for this mirror. The output coupler used for this cavity was a piece of glass that provided approximately 4 percent reflectivity at the front and back surface for a total reflectivity of 8 percent at all laser wavelengths. The distance between the output coupler and the highly reflective mirror was 6.4 cm.

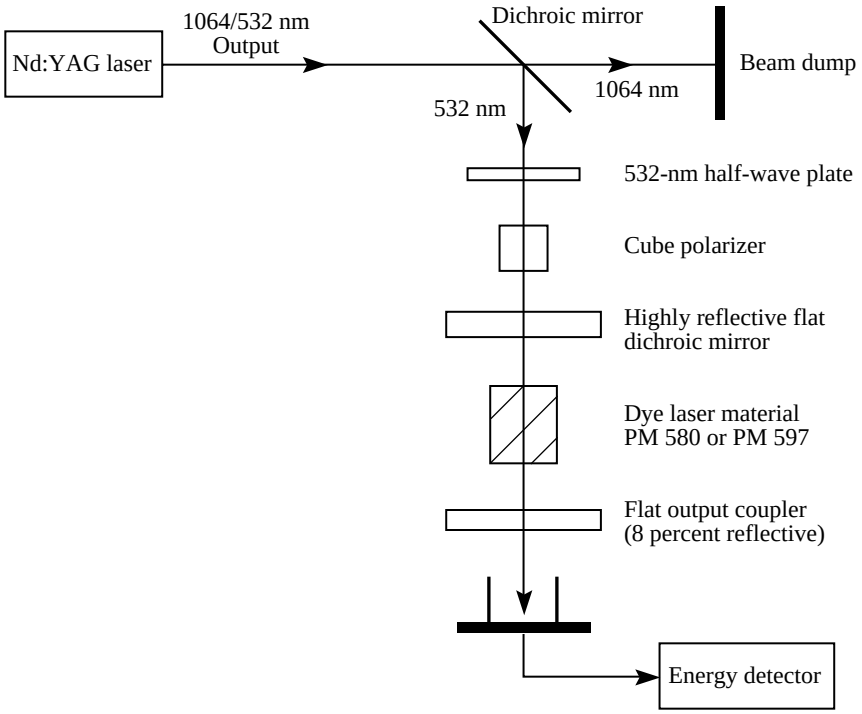

Figure 14. Dye laser oscillator cavity in broadband configuration end pumped by Q-switched Nd:YAG laser.

Table 1. Characteristics of Q-Switched Pulsed Nd:YAG Pump Laser

Wavelength, nm	1064/532
Resonator configuration	Stable
Energy per pulse (maximum), mJ	100
Energy drift, percent	<10
Polarization	Vertical
Repetition rate (maximum), Hz	10
Pulse width, nsec	10–17
Transverse modes	Multiple
Beam diameter at FWHM, mm	6
Divergence, mrad	1.5
Primary power source, V AC	110
Power consumption, amp	<10

The solid-state dye laser materials used as the gain medium for this cavity were pyrromethene laser dyes PM 580 and PM 597 doped in a polymeric host material. The PM 580 laser dye was incorporated in a host material of PMMA using a polymerization process developed by Agilase Inc. The dye host material was prepared from a molar of 1×10^{-4} of the PM 580 laser dye and cut into squares with dimensions $25.4 \times 25.4 \times 12.7$ mm. Both surfaces of the dye material were polished to a high optical quality for optimum laser performance.

The PM 597 dye was in a host material of MPMMA and was manufactured by GosNIIMedpolymer in Moscow, Russia. This modified host material consisted of the same basic chemicals as the PMMA material but includes copolymers and additives to improve the damage resistance to high-intensity pump lasers. The dye host material was prepared from molars of 1×10^{-4} and 2×10^{-4} of the PM 597 laser dye and cut into a 2.54-cm-diameter rod with thicknesses of 10.5, 12.7, and 15 mm. Both the

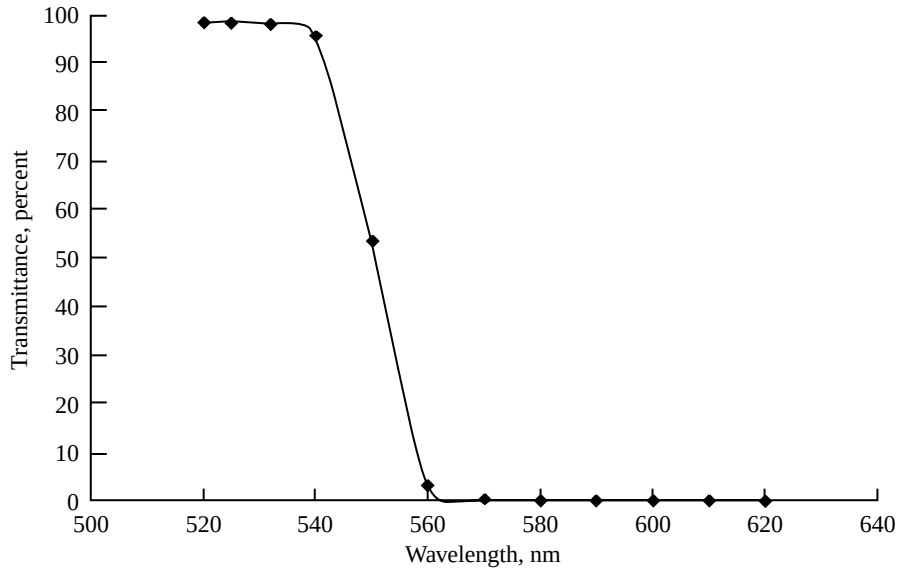

Figure 15. Transmission curve for highly reflective mirror used in broadband dye laser oscillator cavity.

PM 580 and PM 597 dye laser materials were placed in the center of the two mirrors to complete the broadband oscillator cavity.

A helium neon laser was used to align the oscillator cavity for maximum performance at the peak dye laser wavelength. The lasing wavelengths of the oscillator cavity were obtained by using a spectrometer equipped with a charge coupled device (CCD) detector and installed in a personal computer. The spectrometer was calibrated by using a low-pressure mercury lamp. The energy measurements for both the pump laser and dye laser were recorded with either an analog energy meter or a digital energy meter. Laser pulse widths were recorded with a high-speed photodetector connected to a 100-MHz digital oscilloscope.

3.2. Narrowband Laser Cavity Configuration

In order to improve the spectral characteristics of the solid-state dye laser and provide tunability in the wavelength region of interest, three SF-10 prisms were placed inside the broadband oscillator cavity. The prisms allow both line narrowing and tunability of the laser beam produced by the solid-state dye laser material. The experimental setup for this configuration is shown in figure 16.

The narrowband oscillator cavity was collinearly end pumped by the same Q-switched pulsed Nd:YAG laser used in the broadband configuration. Because the SF-10 prisms must accept only horizontally polarized light, a half-wave plate was placed outside the cavity to rotate the polarization of the pump beam from vertical to horizontal. A plano-convex lens was used to reduce the size of the pump beam so that higher order transverse modes are not excited by the pump laser beam. A beam profile instrument was used to examine the beam characteristics of the dye laser output. The dye laser material was rotated to Brewster angle to reduce the reflections caused by the flat polished surfaces of the dye material. The output coupler was a flat mirror with a coating that was 10 percent reflective at 600 nm on the mirror side, and antireflective coated for the visible laser wavelengths on the opposite side. This mirror also had a 2° wedge on the backside to reduce the internal reflections in the oscillator cavity. A concave dielectric-coated mirror that passed 95 percent of the pump laser beam while having a reflectivity greater than 95 percent between 580 and 630 nm was used as the highly reflective mirror. This

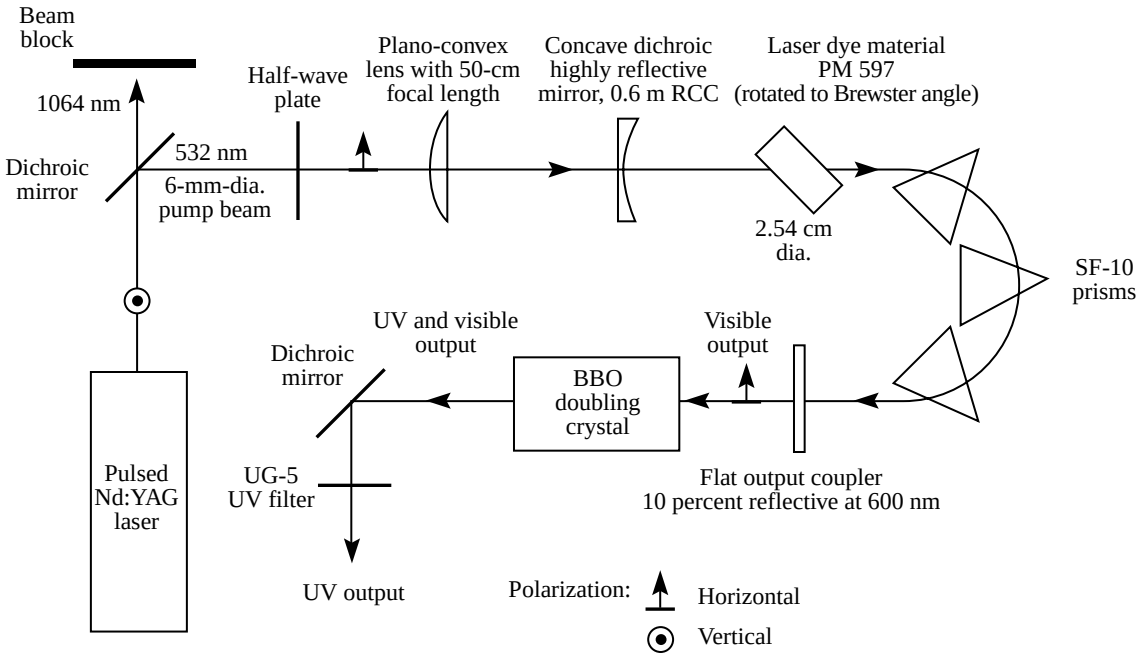

Figure 16. Dye laser oscillator cavity in narrowband configuration end pumped by Q-switched Nd:YAG laser.

mirror was used in the narrowband configuration to provide a more stable oscillator cavity. The total length of the cavity was 38 cm.

To extend the wavelength of the dye laser oscillator output into the UV region, a BBO nonlinear optical crystal with dimensions $10 \times 10 \times 5$ mm was used for second harmonic generation. This crystal was chosen because of its wide transmission region and large angle tuning range for phase matching. The BBO crystal also has a high damage threshold and a broad temperature acceptance bandwidth. Some of the optical properties of this material are shown in table 2. This crystal was used with the narrowband configuration of the dye laser oscillator to produce a wavelength of 289 nm, which corresponds to the on-line wavelength used for atmospheric measurements of ozone in the DIAL laser system.

Table 2. Nonlinear Optical Properties for Type I BBO Crystal

Size of crystal, mm	$10 \times 10 \times 5$
Spectral acceptance, nm	189–1750
Refractive indices at—	
1.0642 μm	$n_e = 1.5425$, $n_o = 1.6551$
0.5321 μm	$n_e = 1.5555$, $n_o = 1.6749$
0.2660 μm	$n_e = 1.6146$, $n_o = 1.7571$
Damage threshold at—	
1.064 μm, GW/cm^2 (10 ns)	5
0.532 μm, GW/cm^2 (10 ns)	1
0.266 μm, MW/cm^2 (8 ns)	120
Nonlinear coefficients	$d_{11} = 5.8d_{36}$ (KDP)
	$d_{31} = .05d_{11}$
	$d_{22} < .05d_{11}$
Acceptance angle, mrad-cm	1.0
Walk-off angle, deg	3.2
Temperature acceptance, deg	51

To separate the visible wavelength from the UV output of the doubling crystal, a dichroic mirror and a UV transmitting filter were used. The dichroic mirror was coated to transmit 85 percent of visible wavelengths between 570 and 600 nm and to reflect more than 99 percent of the wavelengths in the UV region from 200 to 300 nm at an angle of incidence of 45°. A UV transmitting glass filter was used to block the residual visible wavelength from the doubling crystal. This filter transmitted more than 87 percent of wavelengths from 250 to 330 nm. The digital energy meter was placed at the output of the filter to measure the UV energy from the BBO doubling crystal.

4. Solid-State Dye Laser Experimental Results

The experimental results from both the broadband and narrowband laser cavity configurations of the solid-state dye laser are discussed in this section. First, the laser threshold, conversion efficiency, and lifetime measurements are discussed. Second, the experimental measurements of tunability, beam divergence, and line width of the narrowband laser cavity are then discussed to determine the second harmonic conversion efficiency. Finally, the experimental and theoretical results of the second harmonic conversion efficiency are compared.

4.1. Experimental Results From Broadband Oscillator Cavity

4.1.1. Laser Threshold Measurements

The lasing spectrum of the broadband oscillator cavity with the experimental setup of figure 14 was measured near the laser threshold for both the PM 580 and PM 597 dye materials at a thickness of 12.7 mm. The total length of the cavity was 6 cm. The input energy to the oscillator was measured with the energy meter, which was placed at the output of the half-wave plate and cube polarizer. The output energy was directed into a fiber-optic cable for a measurement of the lasing spectrum. Figure 17 shows

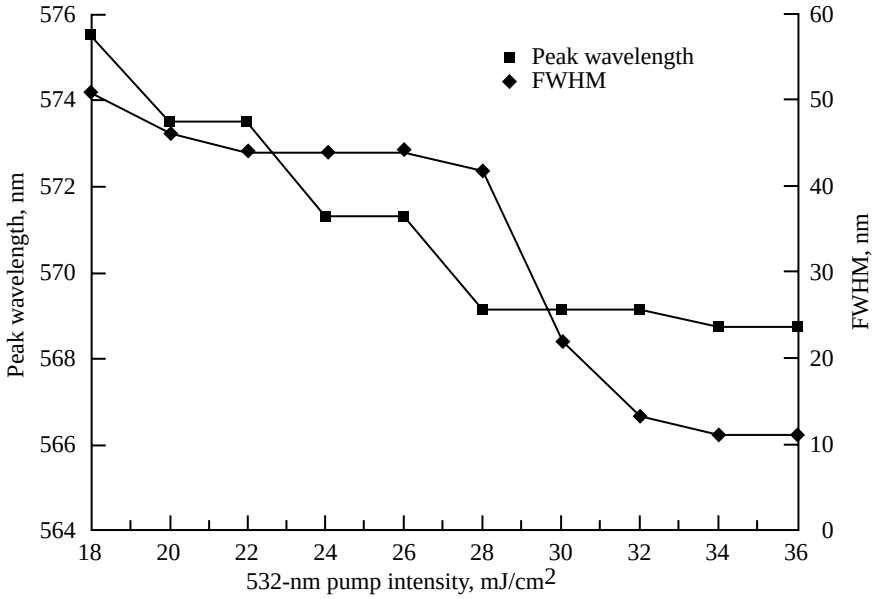

Figure 17. Peak laser wavelength and bandwidth of PM 580 dye material at molar of 1×10^{-4} and thickness of 12.7 mm as function of pump intensity.

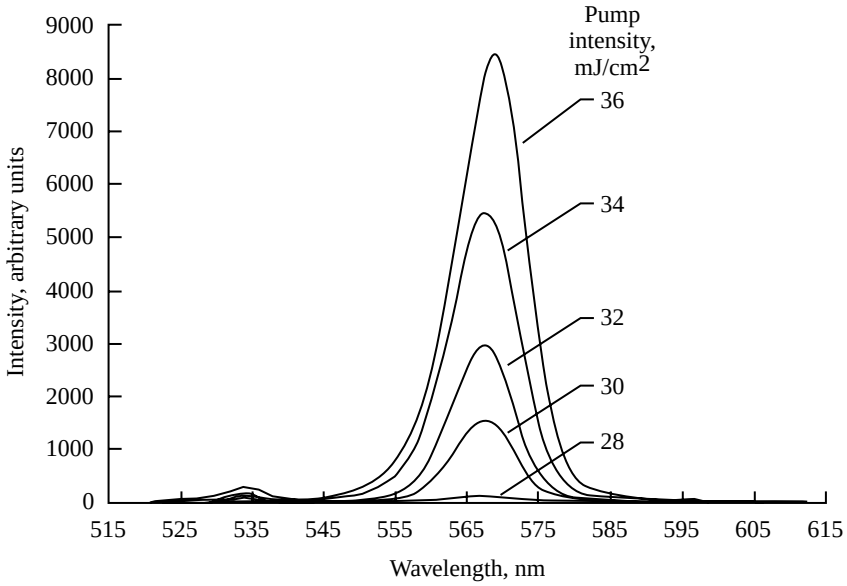

Figure 18. Laser spectra of broadband oscillator cavity at various pump intensities near laser threshold for PM 580 laser dye material.

the peak wavelength and the full width at half maximum (FWHM) bandwidth for the PM 580 dye material (molar of 1×10^{-4}) as a function of the pump intensity. The peak wavelength was measured by calculating the average of the data points from the base to the peak of the laser cavity output spectra shown in figure 18. A line was drawn in the middle of the spectra to connect the averaged points and to determine the wavelength at the peak of the laser spectra. At lower intensities, the bandwidth of the dye laser was very large due to the spontaneous emission of the laser material. As the pump laser intensity increased, the peak dye laser wavelength shifted toward the pump laser wavelength and the bandwidth decreased. Stimulated emission was reached after a sharp change from 26 to 32 mJ/cm^2. The peak wavelength and bandwidth of the oscillator cavity remained constant at pump intensities beyond the laser threshold intensity of 34 mJ/cm^2.

This experiment was performed twice at each data point shown in figure 17, and the results shown are an average of the two measurements. The manufacturer-stated pulse-to-pulse stability of the Nd:YAG pump laser was ±6 percent rms. The pulse-to-pulse stability of the dye laser was found by observing the output of the oscillator cavity with an oscilloscope. The average output of the dye laser was taken after 100 pulses and the stability was found to be ±11 percent of the average output.

The spectral output of the oscillator cavity was measured at various pump intensities near the laser threshold and is shown in figure 18. The observation was that the PM 580 dye material did not absorb all the 532-nm pump laser beam.

The same experiment was performed with the PM 597 dye material (molar of 1×10^{-4}) at a thickness of 12.7 mm. The experiment was performed twice at each data point shown in figure 19, and the results shown are an average of the two measurements. The pulse-to-pulse stability of the dye laser was found by observing the output of the oscillator cavity with an oscilloscope. The average output of the dye laser was taken after 100 pulses and the stability was found to be ±11 percent of the average output. The peak wavelength was measured by calculating the average of the data points from the base to the peak of the laser cavity output spectra shown in figure 20. A line was drawn in the middle of the spectra to connect the averaged points and to determine the wavelength at the peak of the laser spectra. Smaller

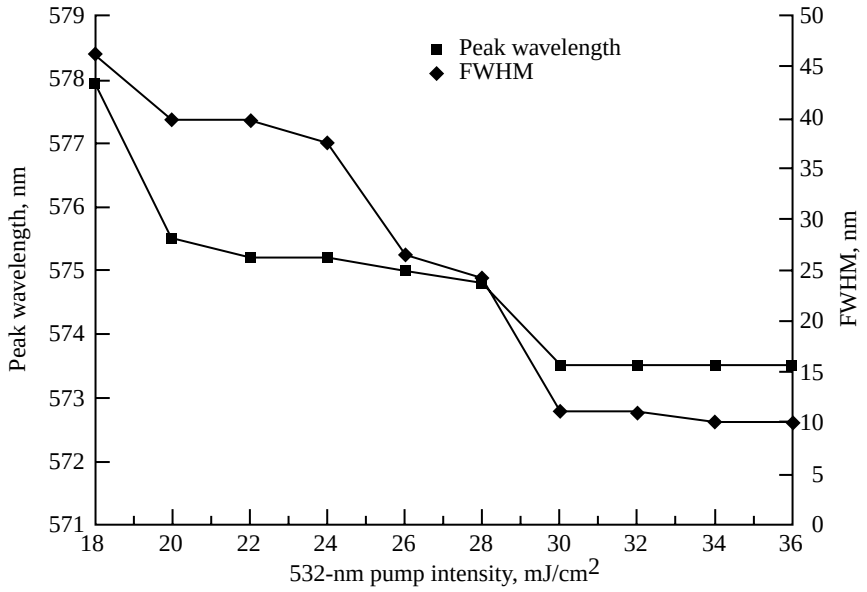

Figure 19. Peak laser wavelength and bandwidth of PM 597 dye material at molar of 1×10^{-4} and thickness of 12.7 mm as function of pump intensity.

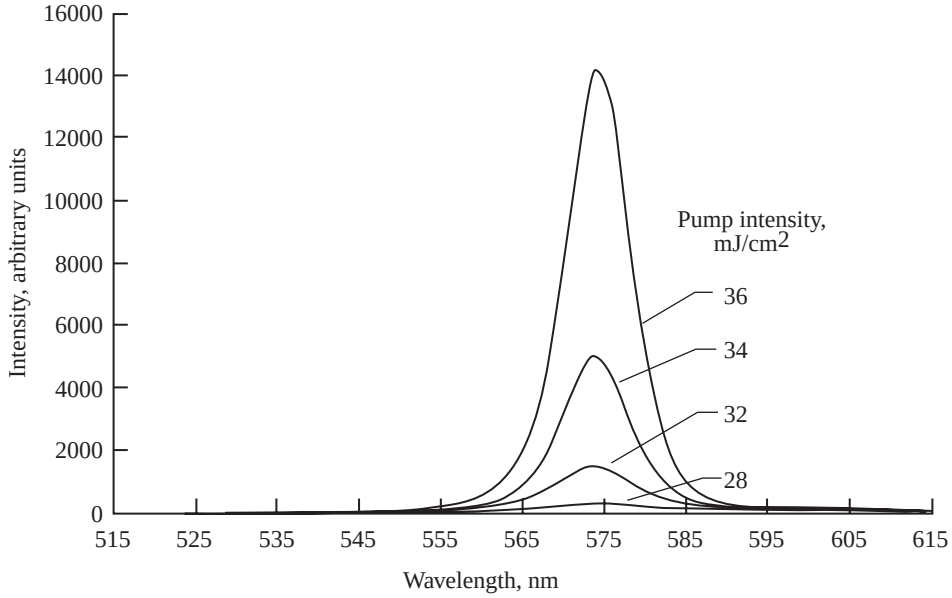

Figure 20. Laser spectra of broadband oscillator cavity at various pump intensities near laser threshold for PM 597 laser dye material.

changes were in the peak wavelength, but the bandwidth of the laser output was almost the same as that measured with the PM 580 dye material. The peak laser wavelength and the bandwidth remained constant at input intensities beyond 31 mJ/cm^2. Unlike the PM 580, the PM 597 dye material absorbed all the 532-nm pump laser energy near the laser threshold. The spectral response of this dye material is shown in figure 20 at various pump intensities. The peak laser wavelength of the PM 597 dye material was 573 nm, which is shifted to a longer wavelength compared with the peak wavelength of the PM 580 dye material.

4.1.2. Laser Efficiency Measurements

The laser efficiency of both the PM 580 and PM 597 solid-state dye materials at a molar of 1×10^{-4} and thickness of 12.7 mm was measured to compare the performance of each in the broadband oscillator configuration shown in figure 14. For this experiment, the oscillator cavity length was 6 cm and remained the same length for both dye materials throughout the experiment. The oscillator cavity was aligned by using the helium neon laser, and the Nd:YAG laser was used to pump the cavity at a repetition rate of 10 Hz. The input energy to the oscillator was measured at the output of the cube polarizer. The energy meter was then removed and the output energy of the dye laser was measured with the digital energy meter within a period of 30 sec to avoid damaging the laser dye molecules inside the host material at high input energy levels. Once the output energy measurement was made, the input energy was measured and increased to a higher level by increasing the energy of the Nd:YAG pump laser. This process was repeated several times until the maximum pump output energy (≈100 mJ) was reached with the Nd:YAG laser. The output energy of the oscillator cavity was measured from the lowest to the highest input energy at the same pump laser spot on the dye material. This experiment was repeated for both the PM 580 and PM 597 dye laser materials, and the output energy of the oscillator cavity was measured from the highest to the lowest pump input energy of the Nd:YAG laser.

The slope efficiency defined as the ratio of the output laser energy to the input energy of the pump laser was calculated by using the least-squares fitting approach to the slope of a line for all data points. The results of the slope efficiency measurements for the PM 580 and PM 597 dye laser materials at a molar of 1×10^{-4} and thickness of 12.7 mm are shown in figures 21 and 22. The slope efficiency was calculated after the dye laser became stable at a pump input energy above the threshold for lasing. The PM 580 dye showed a slope efficiency of 67 percent initially but dropped to a value of 66 percent when the experiment was performed for a second time. The PM 597 dye material showed an improved slope efficiency performance of 79 percent under the same testing conditions but did not drop significantly in the output energy when performing the experiment for a second time.

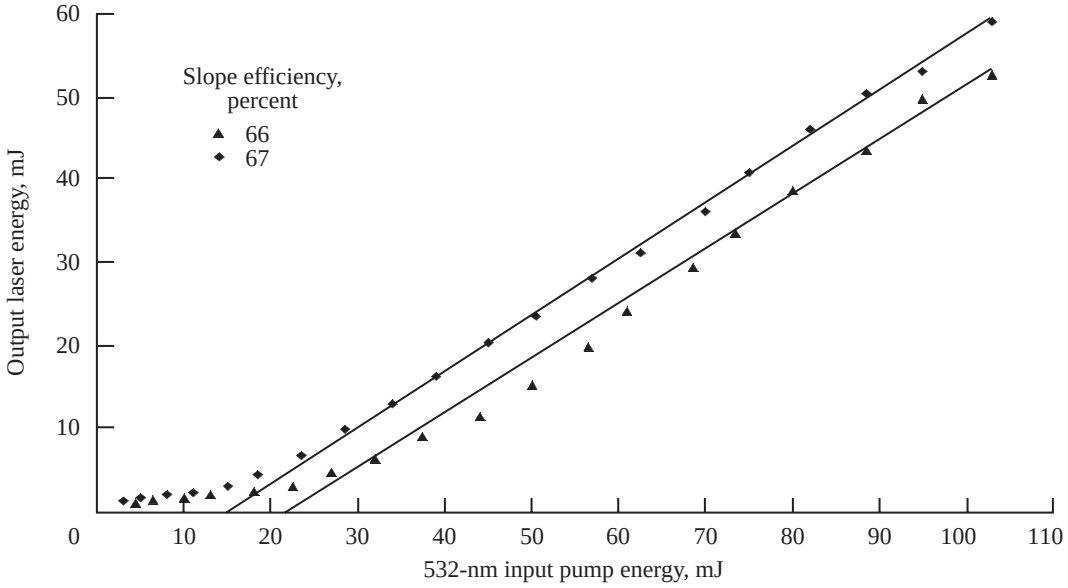

Figure 21. Two measurements of slope efficiency for PM 580 dye laser material at molar of 1×10^{-4} and thickness of 12.7 mm in broadband oscillator cavity.

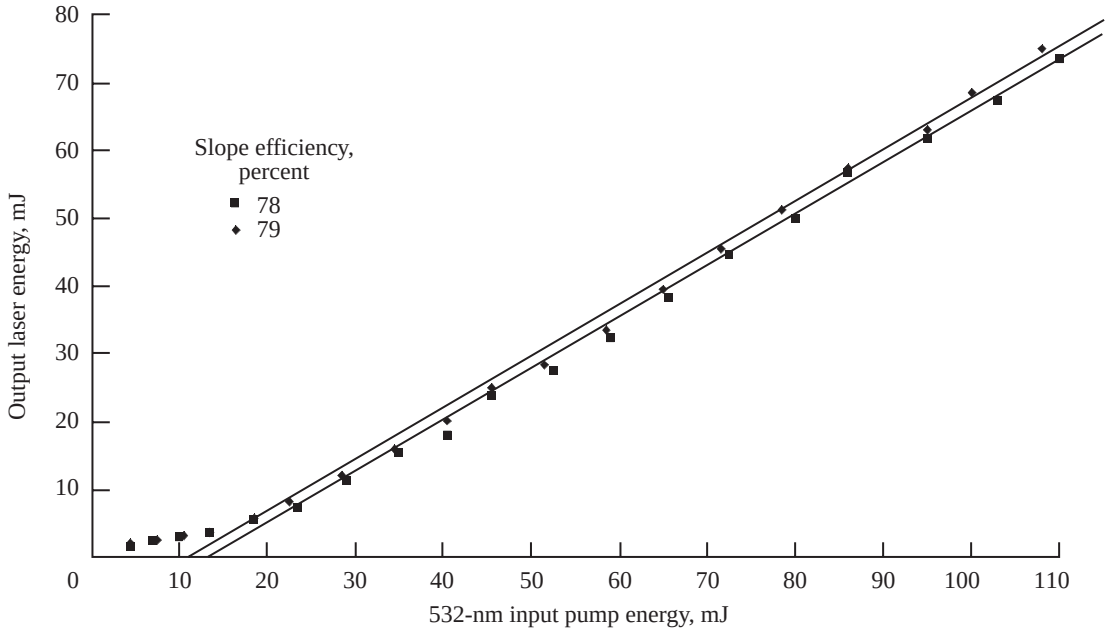

Figure 22. Two measurements of slope efficiency for PM 597 dye laser material at molar of 1×10^{-4} and thickness of 12.7 mm in broadband oscillator cavity.

The PM 580 laser dye doped in the PMMA host material showed optical damage at the pump laser spot after the experiment was completed. The PM 597 laser dye doped in the MPMMA host material showed no optical damage, but a transparent region was seen at the pump laser spot where the laser dye was depleted. This improved performance of the PM 597 laser dye is primarily due to the damage resistant modifications to the PMMA host material.

4.1.3. Lifetime Measurements

The useful service lifetime of solid-state dye materials when pumped by a pulsed laser source is an important property to consider for practical use in an ozone DIAL laser system. For remote sensing applications, operating the laser transmitter continuously for an extended period of time (>36 000 laser shots) to collect data over large regions of the atmosphere would be desirable. To determine the service lifetime of both the PM 580 and PM 597 dye materials, the broadband oscillator cavity was used in the same configuration shown in figure 14. Three different pump energies were used for both dye materials ranging from a low- to a high-intensity level. For each level of intensity, the pump energy remained constant at a pulse repetition rate of 10 Hz and was terminated after the dye laser energy dropped by 50 percent of the initial value. The lifetime performance of the PM 580 dye material (molar of 1×10^{-4}) with a thickness of 12.7 mm at an input intensity of 0.1 J/cm^2 is shown in figure 23. The efficiency of the dye material in figure 23 is defined as the ratio of the dye laser output energy to the input energy of the pump laser. The dye laser output energy dropped 50 percent of the initial value after approximately 90 000 laser shots. This experiment was performed once and the data points were collected after a period of approximately 3000 laser shots. The pulse-to-pulse stability of the Nd:YAG pump laser was ±6 percent rms, whereas the dye laser stability was found to be ±11 percent of the average output from the oscillator cavity after 100 pulses.

The lifetime performance of the PM 597 dye material under the same test conditions is shown in figure 24. The experiment was performed once and the data points were collected after a period of approximately 3000 laser shots. The pulse-to-pulse stability of the Nd:YAG pump laser was ±6 percent rms, whereas the dye laser stability was found to be ±11 percent of the average output from the

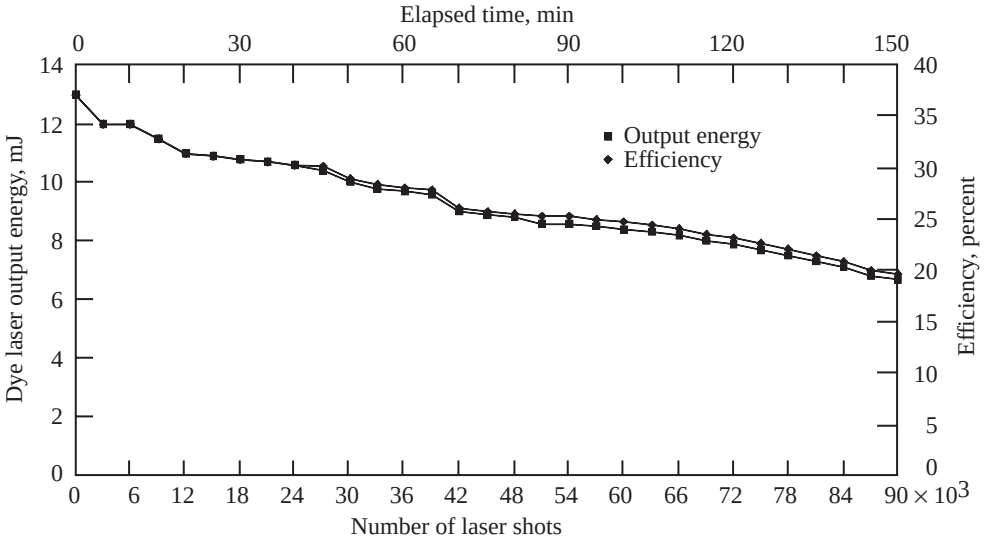

Figure 23. Lifetime performance of PM 580 dye material (molar of 1×10^{-4}) at thickness of 12.7 mm. Nd:YAG pump laser operated at repetition rate of 10 Hz with intensity of 0.1 J/cm^2.

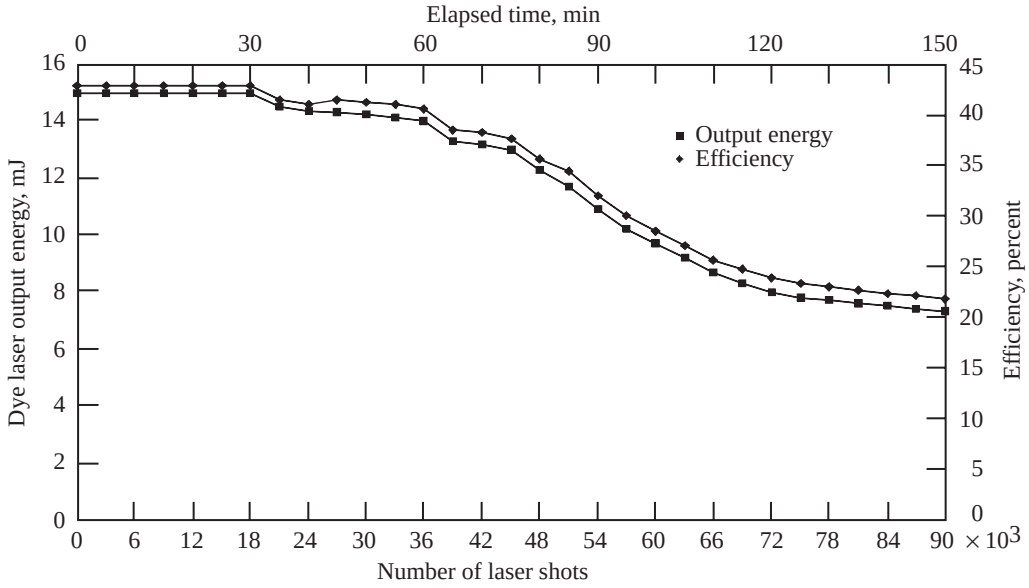

Figure 24. Lifetime performance of PM 597 dye material (molar of 1×10^{-4}) at thickness of 12.7 mm. Nd:YAG pump laser operated at repetition rate of 10 Hz with intensity of 0.1 J/cm^2.

oscillator cavity after 100 pulses. The PM 597 dye material maintained a constant energy output for a 30-min period at the beginning of the experiment unlike the PM 580 dye material, which showed a decline in the output energy immediately after starting the experiment. Both dye materials lost 50 percent of their original energy output after 2 1/2 hr of continuous operation at 10 Hz. At higher intensity levels, the lifetime performance for both materials was significantly reduced. The lifetime performance of the PM 580 and PM 597 dye laser materials at a molar of 1×10^{-4} and thickness of 12.7 mm is shown in figure 25 at various pump laser intensities. The output energy of the PM 597 dye material remained constant after a 15-min period but dropped sharply after 30 min at a pump laser intensity of 0.5 J/cm^2. The output energy of the PM 580 dye material dropped 50 percent of its initial value after only

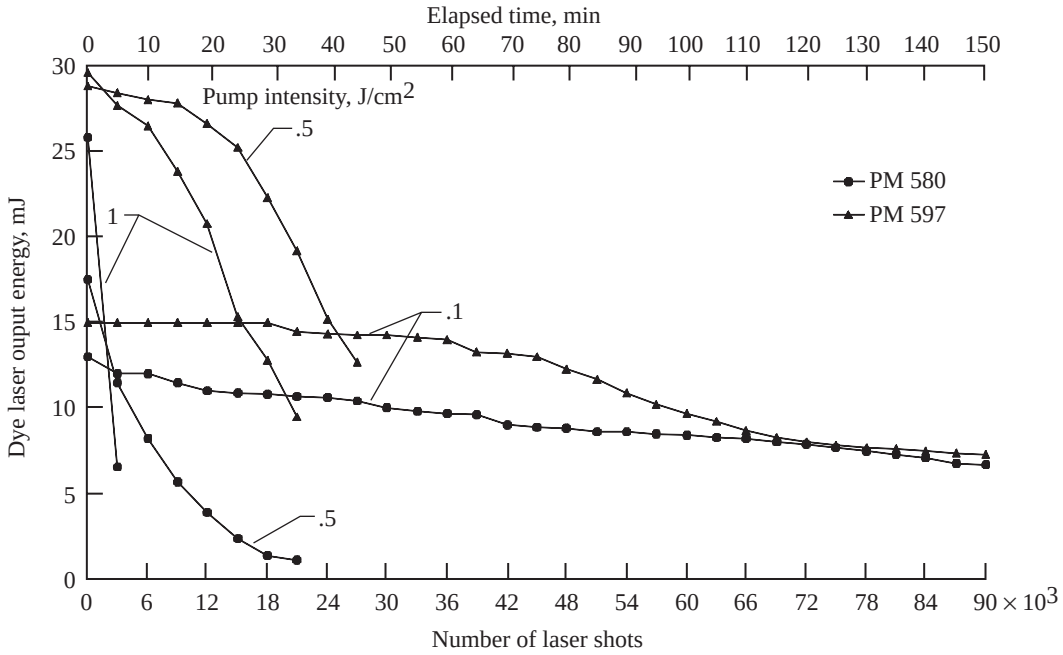

Figure 25. Lifetime performance of PM 580 and PM 597 dye materials (molar of 1×10^{-4}) at thickness of 12.7 mm. Nd:YAG pump laser operated at repetition rate of 10 Hz with intensities of 0.1, 0.5, and 1 J/cm^2.

10 minutes of operation due to optical damage at the surface of the material. The fastest destruction of the dye molecules occurred in both materials at an input intensity of 1 J/cm^2.

In addition to measuring the output energy, the spectral content of the dye laser was measured with the spectrometer at different times during the same experiment. The lasing spectra of the oscillator cavity for the PM 580 dye laser material at a pump laser intensity of 0.1 J/cm^2 are shown in figure 26. The initial measurement is taken at the beginning of the experiment, and the final measurement is taken after the dye laser output energy dropped by 50 percent of the original value. A shift in the peak wavelength toward the UV region and an increase of the pump laser intensity at 532 nm was observed over the period of the test. This change in absorption of the dye material at the pump wavelength may be due to the "bleaching" or damage to the dye molecules in the area of the laser pumping. The PM 597 dye material showed a similar shift in the peak wavelength during the lifetime tests as shown in figure 27. A larger shift occurred in the peak wavelength of the PM 580 dye material at the end of the lifetime test in comparison with the PM 597 dye material under the same conditions.

To measure the amount of the 532-nm pump laser energy that was unabsorbed by the dye material, an interference filter was placed at the output of the oscillator cavity. The interference filter was used to transmit only the pump laser wavelength (532 nm) and to absorb the dye laser wavelengths. The energy of the pump laser unabsorbed by the dye material at an input intensity of 0.1 J/cm^2 was measured for both the PM 580 and the PM 597 dye laser materials with the energy meter, and the results are shown in figure 28. At an input intensity of 0.1 J/cm^2, the percentage of pump energy absorbed by both dye laser materials was measured. A steady decrease occurred in the absorption of the pump laser energy after a period of 30 min due to the damaging effects of the pump laser on dye molecules inside the host material. This change in absorption also contributes to the shift in the dye laser wavelength towards the 532-nm pump laser wavelength. The efficiency defined as the ratio of converted energy to that absorbed for both dye materials remained approximately constant throughout the operating lifetime and is shown in figure 29.

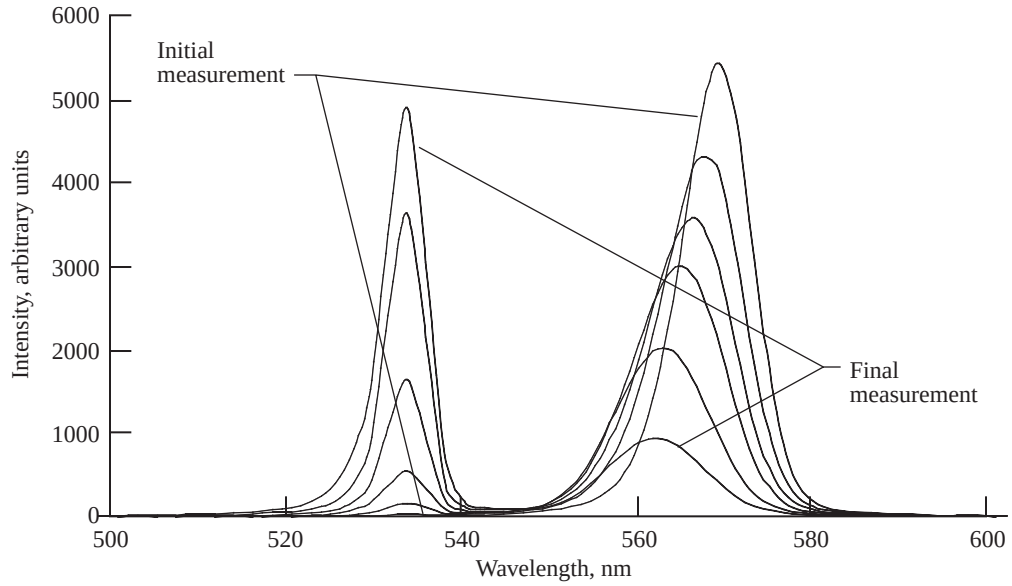

Figure 26. Spectral content of PM 580 dye material (molar of 1×10^{-4}) at thickness of 12.7 mm at beginning and end of lifetime measurement. Nd:YAG pump laser operated continuously at repetition rate of 10 Hz at intensity of 0.1 J/cm^2.

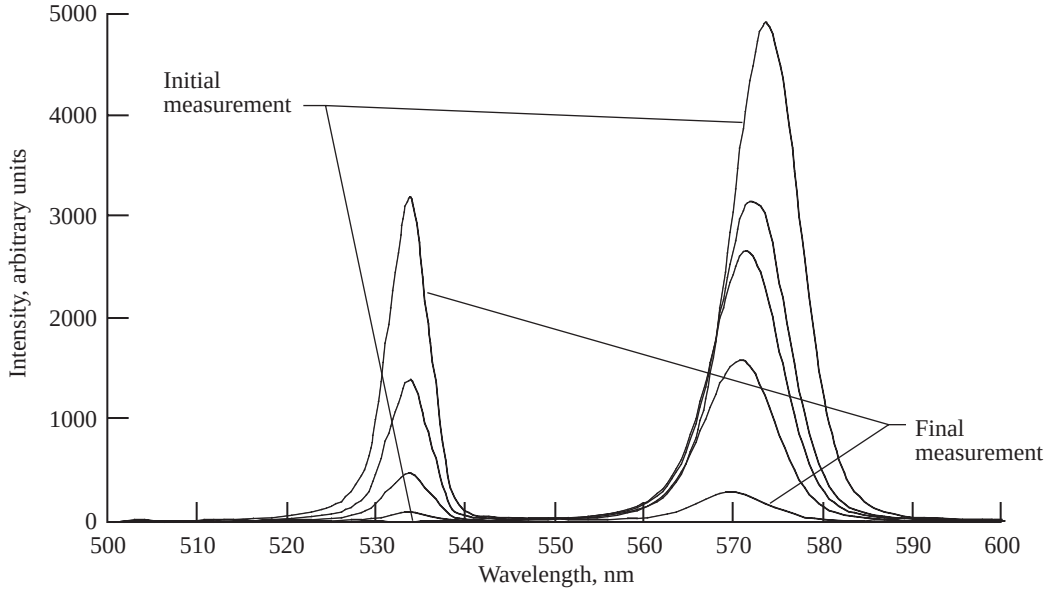

Figure 27. Spectral content of PM 597 dye material (molar of 1×10^{-4}) at thickness of 12.7 mm at beginning and end of lifetime measurement. Nd:YAG pump laser operated continuously at repetition rate of 10 Hz at intensity of 0.1 J/cm^2.

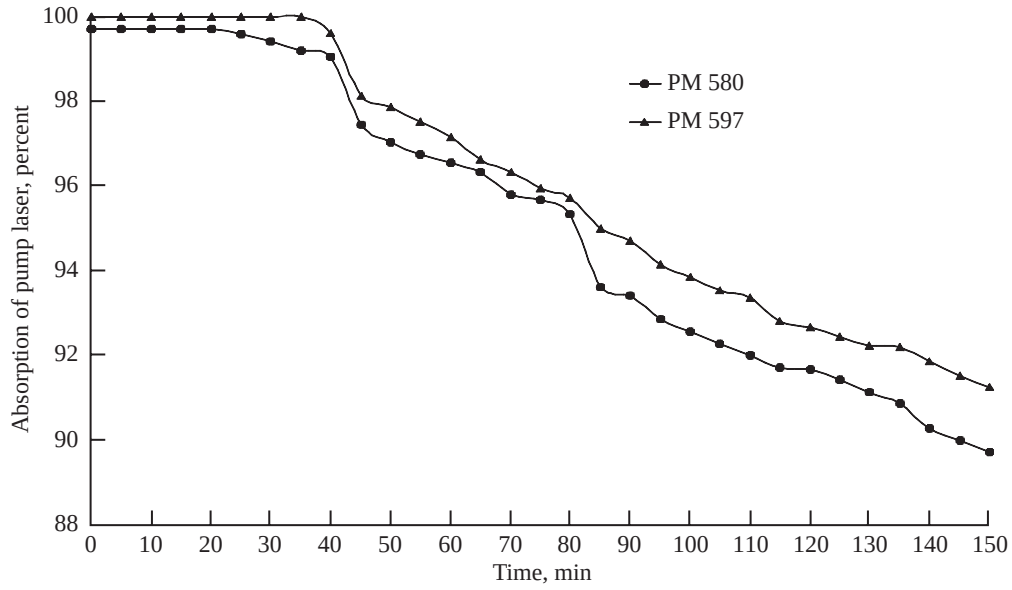

Figure 28. Pump laser energy absorbed by PM 580 and PM 597 dye materials at input intensity of 0.1 J/cm^2 expressed as percentage over period of lifetime measurement.

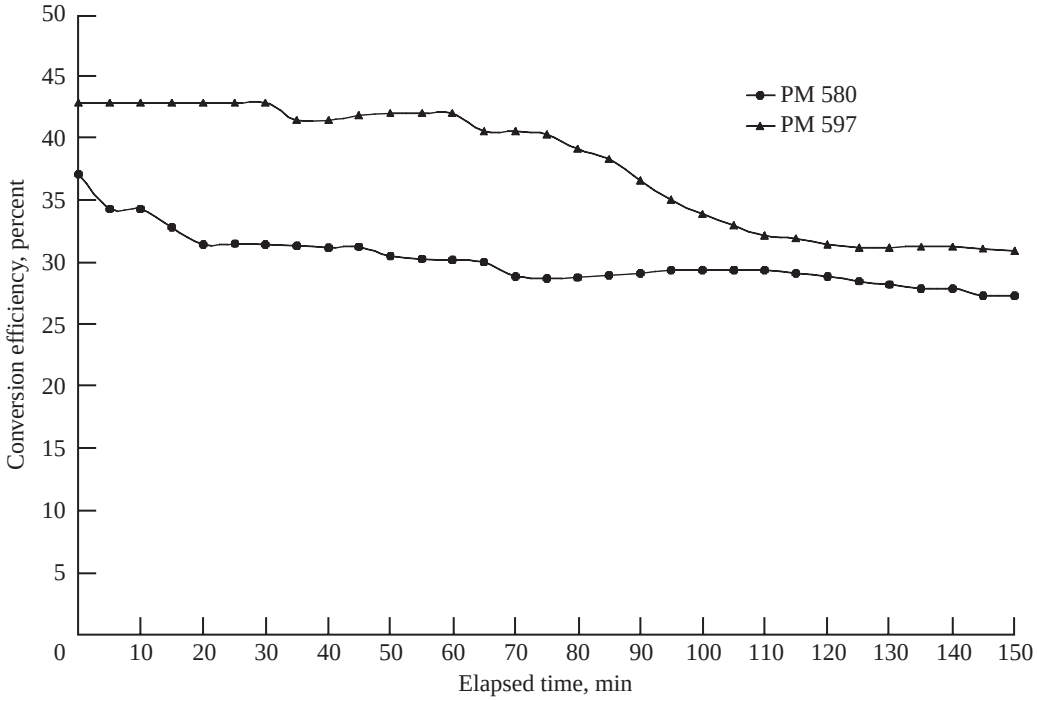

Figure 29. Efficiency of PM 580 and PM 597 dye materials defined as ratio of converted energy to that absorbed over period of lifetime measurement.

4.2. Experimental Results From Narrowband Oscillator Cavity

4.2.1. Laser Efficiency Measurements

The laser efficiency of the PM 597 solid-state dye material was measured in the narrowband configuration as shown in figure 16 because of its improved performance in comparison with the PM 580 solid-state dye materials in the broadband configuration. For this experiment, the oscillator cavity length was 38 cm and remained the same length throughout the experiment. The focusing lens outside of the oscillator cavity reduced the size of the pump laser beam from 6 to 1 mm in diameter (FWHM). The efficiency of the PM 597 dye material was measured at each dye thickness (10.5, 12.7, and 15 mm) to determine which length produced the highest oscillator cavity efficiency. The oscillator cavity was aligned by using the Nd:YAG pump laser at a low energy and a pulse repetition rate of 10 Hz. Once the cavity was aligned, the spectrometer was used to measure the peak laser wavelength at the output of the oscillator cavity. The oscillator cavity was tuned to 578 nm by adjusting the prisms and the output coupler in the horizontal direction. The pulse repetition rate of the Nd:YAG laser remained at 10 Hz throughout the experiment. The input energy to the oscillator was measured at the output of the half-wave plate. The energy meter was then removed and the output energy of the dye laser was measured with the digital energy meter within a period of 30 sec to avoid damaging the laser dye molecules inside the host material. The measurement was repeated at the same input energy level to determine the reproducibility. Once the output energy measurement was made for the second time, the input energy was measured and then increased to a higher level by increasing the energy of the Nd:YAG pump laser. This process was repeated for each data point until the maximum output energy (≈100 mJ) was reached with the Nd:YAG laser. The pulse-to-pulse stability of the Nd:YAG pump laser was ±6 percent rms, whereas the dye laser stability was found to be ±11 percent of the average output from the oscillator cavity after 100 pulses. The results for the molars of 1×10^{-4} and 2×10^{-4} of the PM 597 dye materials at various thicknesses are shown in figures 30 and 31. Each data point reflects the average of the two measurements taken at each input energy level.

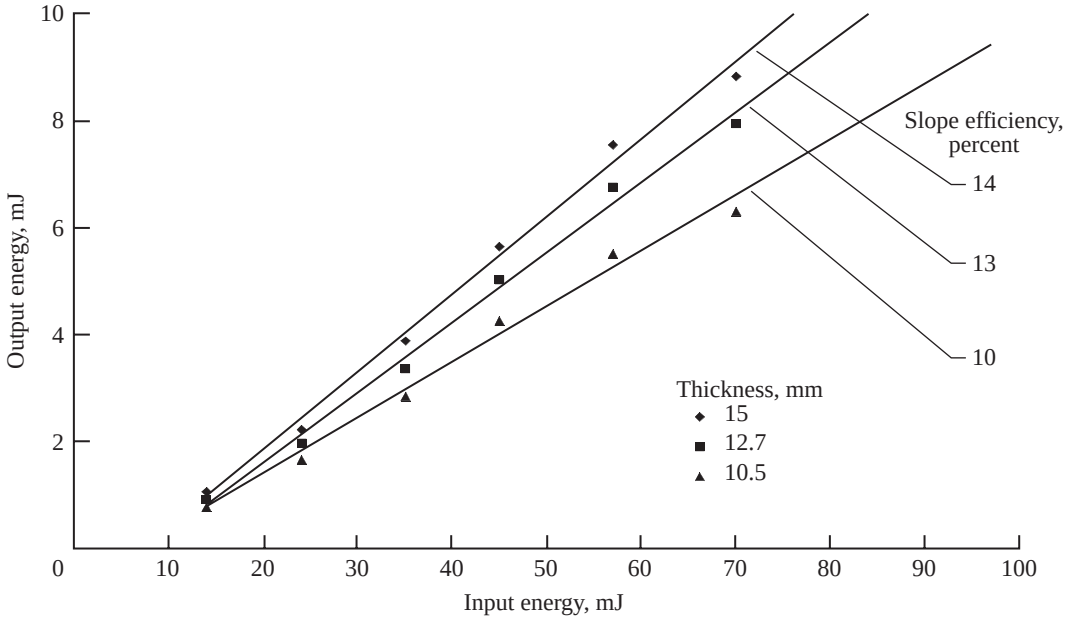

Figure 30. Slope efficiency of PM 597 dye material (molar of 1×10^{-4}) at various lengths in narrowband oscillator cavity.

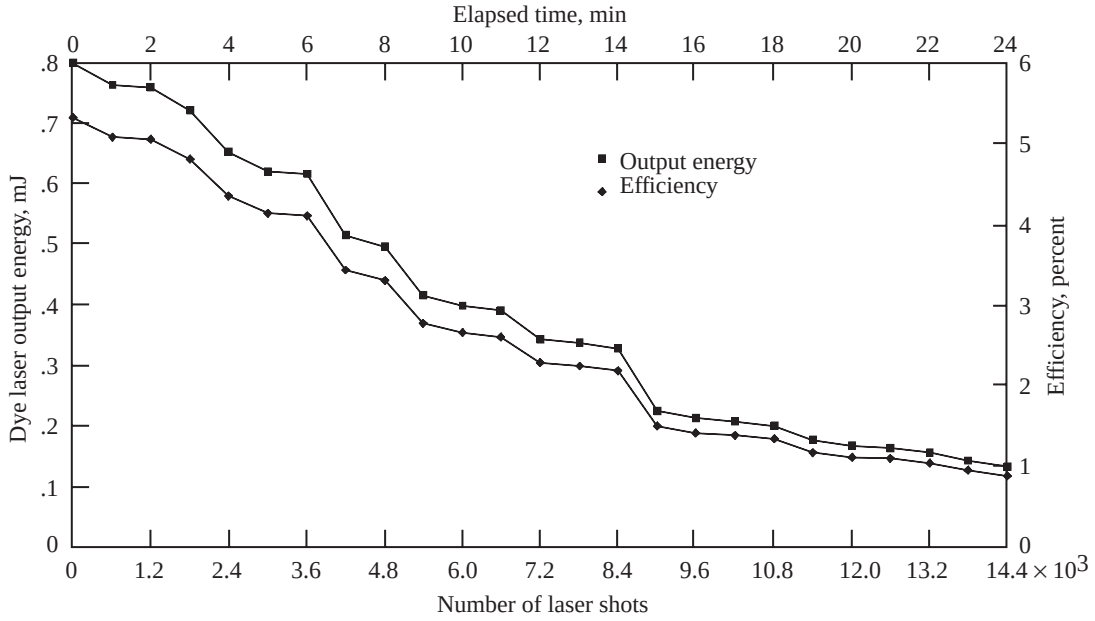

Figure 31. Lifetime performance of PM 597 dye material (molar of 2×10^{-4}) at thickness of 15 mm. Nd:YAG pump laser operated at repetition rate of 10 Hz with intensity of 2 J/cm^2.

The slope efficiency defined as the ratio of the dye laser energy to the pump laser energy was calculated by using the least-squares fitting approach to the slope of a line for all data points. The PM 597 dye material at 15 mm in thickness was observed to show an improvement in the slope efficiency compared with the same dye material at small thicknesses in both the molars of 1×10^{-4} and 2×10^{-4}. The higher concentration of laser dye produced a higher gain in the oscillator cavity which resulted in a higher slope efficiency. The PM 597 dye material at a molar of 2×10^{-4} and thickness of 15 mm was chosen for use in the narrowband oscillator configuration because of the improved slope efficiency performance.

4.2.2. Lifetime Measurements

The lifetime performance of the PM 597 dye material at a molar of 2×10^{-4} and thickness of 15 mm was tested in the narrowband configuration shown in figure 16. Three different input energies were used to test the performance of the dye material ranging from a low- to a high-intensity level. For each level of intensity, the input energy remained constant at a pulse repetition rate of 10 Hz. The lifetime performance of the PM 597 dye material at an input intensity of 2 J/cm^2 is shown in figure 31. The efficiency of the dye material labeled in figure 31 is defined as the ratio of the output energy of the dye laser to the input energy of the pump laser. This experiment was performed once and the data points were collected after a period of approximately 600 laser shots. The pulse-to-pulse stability of the Nd:YAG pump laser was 6 percent rms, whereas the dye laser stability was found to be 11 percent of the average output from the oscillator cavity after 100 pulses. The dye material lost 50 percent of the original output energy after 10 min of continuous operation. The test was terminated after 24 min when the dye laser output energy dropped beyond 80 percent of the original value.

The life performance of the PM 597 dye material at various pump laser intensities is shown in figure 32. A constant decrease in the dye laser output energy occurred immediately after starting the test at a pump intensity of 9 J/cm^2. The dye material lost 50 percent of the original output energy after

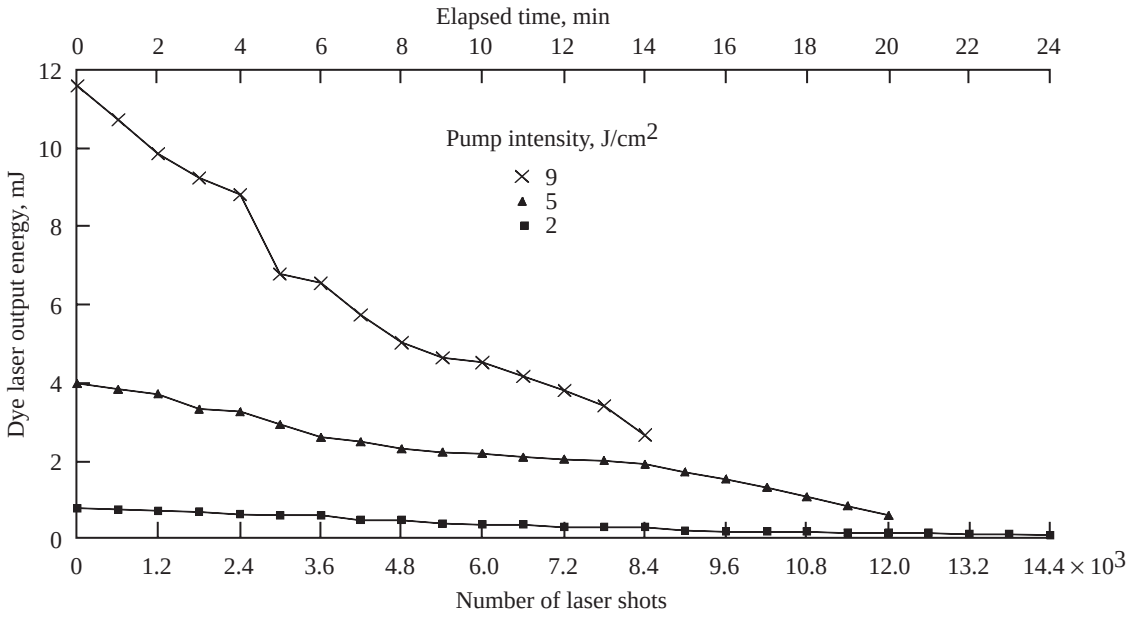

Figure 32. Lifetime performance of PM 597 dye material (molar of 2×10^{-4}) at thickness of 15 mm and pump laser intensities of 2, 5, and 9 J/cm^2.

6 min. The test was terminated after 24 min when the dye laser output energy dropped below 75 percent of the original value. The output energy of the oscillator remained fairly constant throughout the test at a pump laser intensity near threshold. This shows that the damaging effects of the pump laser beam are more apparent at higher energy levels than at lower energy levels.

4.2.3. Tunability

The narrowband oscillator cavity shown in figure 16 provided a wide range of visible laser wavelengths when using the PM 597 dye laser material. This material was chosen because of its fluorescence properties in the visible wavelength region from 550 to 650 nm (ref. 32). The tunability measurement and the fluorescence spectra of the PM 597 dye laser material with a molar of 2×10^{-4} and thickness of 15 mm are shown in figure 33. The lasing spectrum of the oscillator cavity was measured with the spectrometer, and each data point on the tuning curve represents a mechanical tuning of the prisms and output coupler mirror. The tuning curve followed the fluorescence spectra closely at wavelengths between 560 and 600 nm, but the intensity dropped off at wavelengths beyond 600 nm. The peak tuning wavelength of the oscillator cavity was slightly red shifted because of the dielectric coatings on the output coupler and highly reflective mirror. This tuning range is suitable for obtaining both the on- and off-line visible wavelengths (578 and 600 nm) needed for frequency doubling into the UV region. This experiment was performed once and the data points on the tuning curve were collected after a period of approximately 600 laser shots.

4.2.4. Line Width

The three dispersive prisms in the narrowband oscillator cavity of figure 16 were used to reduce the spectral line width of the solid-state dye laser. The line width of the dye laser in the broadband configuration (11 nm) was too large for efficient frequency doubling into the UV region using the BBO doubling crystal. A 1-m scanning monochromator with a resolution of 20 pm was used to measure the line width of the narrowband oscillator cavity. The results of this measurement are shown in figure 34

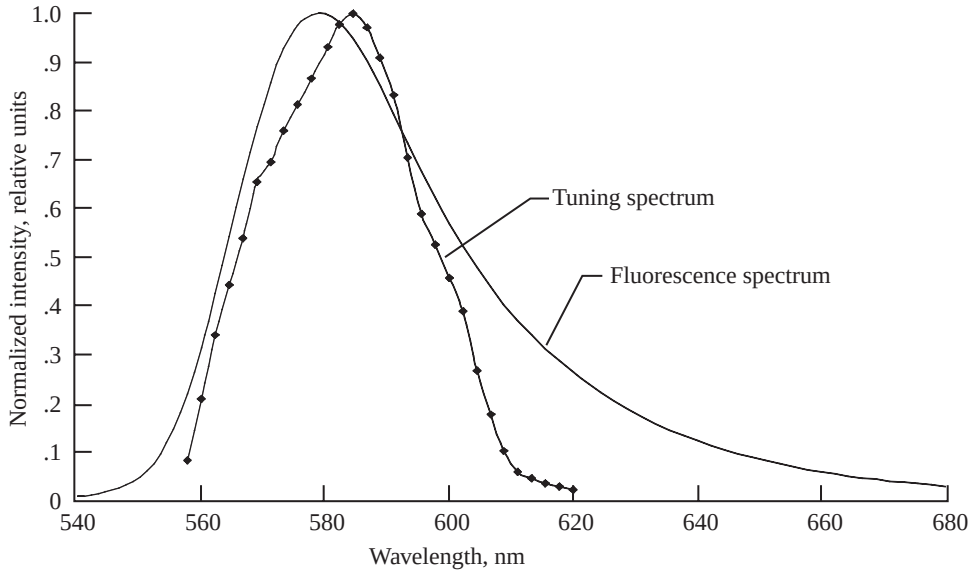

Figure 33. Laser tuning and fluorescence spectra of narrowband oscillator cavity with PM 597 dye material (molar of 2×10^{-4}) at thickness of 15 mm.

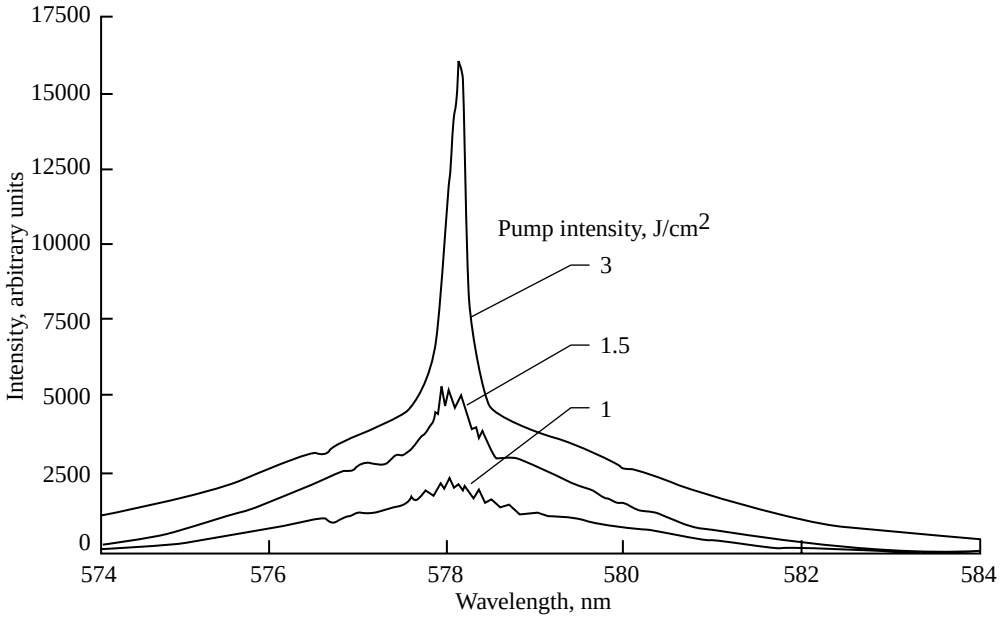

Figure 34. Spectral line width of narrowband oscillator cavity at pump laser intensities of 1, 1.5, and 3 J/cm^2 using PM 597 dye material (molar of 2×10^{-4}) at thickness of 15 mm.

using a molar of 2×10^{-4} for the PM 597 dye material and thickness of 15 mm at pump laser intensities near the laser threshold. At a peak laser wavelength of 578 nm, the line width of the dye laser was measured at full width at half maximum (FWHM). For a low input intensity the line width was greater than 3 nm but narrowed to 370 pm at a pump intensity of 3 J/cm^2. A broad pedestal appeared at the base of the spectrum due to the amplified spontaneous emission created by the dye laser material. This phenomenon has been observed by several authors using similar dye laser materials (refs. 33, 34, and 35). To reduce this effect, the dye laser material was rotated to Brewster angle so that the reflections caused by the flat polished surfaces of the dye material did not contribute to the laser beam. The laser cavity

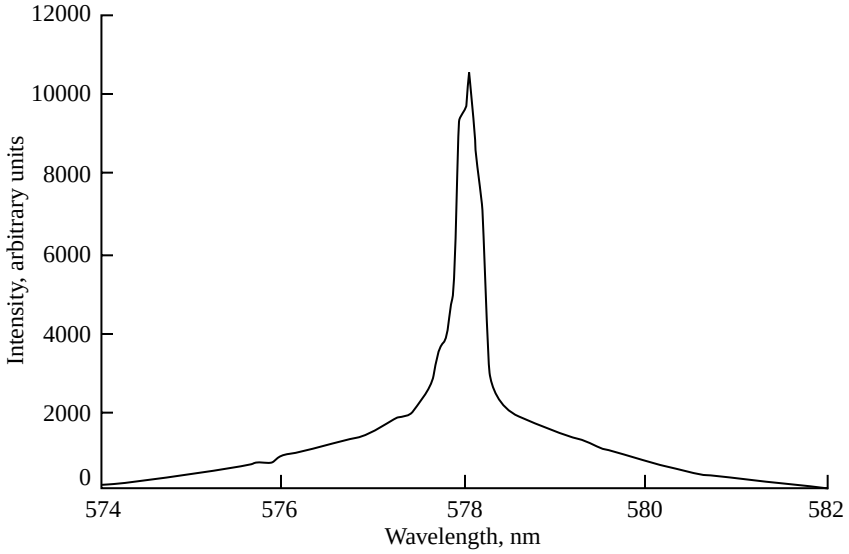

Figure 35. Spectral line width of narrowband oscillator cavity at pump laser intensity of 2 J/cm^2.

mirrors were purchased with antireflective coatings and large wedges to reduce the intercavity reflections. To further reduce the effects of the broad pedestal, the dye laser material was tilted in an upward direction on the optical mount inside the oscillator cavity to suppress the surface reflections that could contribute to the pedestal. Figure 35 shows the line width at a pump laser intensity of 2 J/cm^2 after tilting the dye laser material inside the oscillator cavity. The line width of the dye laser was measured to be 390 pm (FWHM), and the intensity of the pedestal was reduced. The effects of the broad pedestal were further reduced by increasing the intensity of the Nd:YAG pump laser to the maximum of 9 J/cm^2. Figure 36 shows the line width of the narrowband oscillator cavity at a maximum pump laser intensity

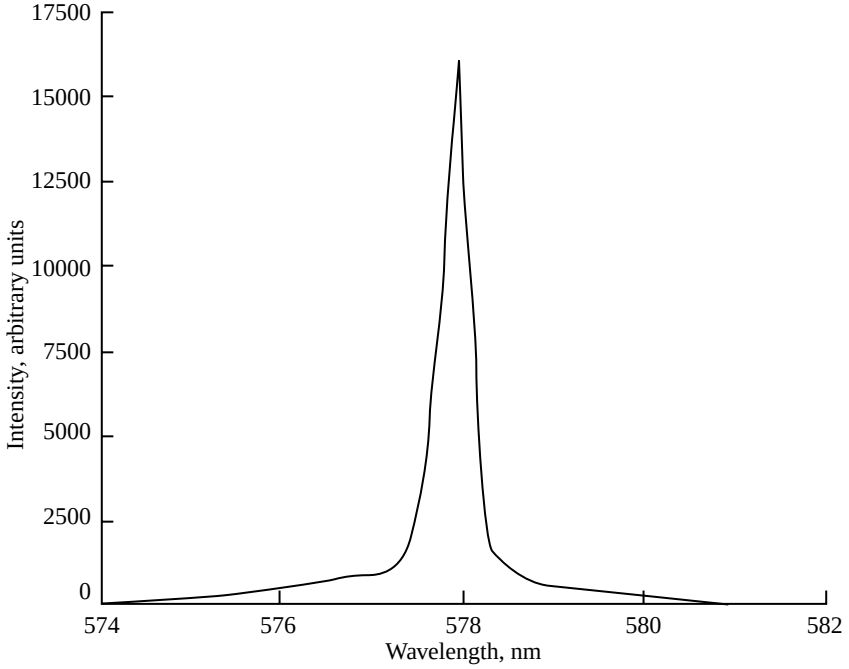

Figure 36. Spectral line width of narrowband oscillator cavity at pump laser intensity of 9 J/cm^2.

of 9 J/cm^2. The line width of the dye laser was measured to be 390 pm (FWHM). The ratio of the intensity contained in the area under the broad pedestal shown in figure 36 to the area under the central spike was estimated to be 23 percent. This shows that the broad pedestal is consuming 23 percent of the total energy of the line-width measurement. The portion of the energy contained in the central spike is more efficiently converted into the UV region with the BBO doubling crystal.

4.2.5. Beam Divergence

A laser beam that exhibits a small divergence is very important for efficient frequency doubling. The beam divergence of the narrowband oscillator cavity with the PM 597 dye laser material (molar of 2×10^{-4}) with a thickness of 15 mm was measured by focusing the dye laser beam into the detector of the beam profile meter by using a convex lens with a focal length of 1 m. The dye laser beam was increased to a maximum energy (≈11 mJ) by maximizing the output energy of the pump laser at a repetition rate of 10 Hz. The diverging laser beam was focused into the detector of the beam profile meter 2 m away from the output of the oscillator cavity by using the convex lens with a focal length of 1 m. The detector was placed at the focal point of the convex lens to measure its diameter. The full angle beam divergence was calculated by dividing the focal spot diameter of the dye laser beam by the lens focal length of 1 m. The divergence of the oscillator cavity improved when the distance between the highly reflective mirror and the dye material increased as shown in table 3. The oscillator cavity showed an improvement in divergence at a longer length because of the change in the beam radius of the fundamental mode at the output coupler. The beam radius of the fundamental mode at the output coupler increased as the cavity length increased and improved the full angle divergence of the oscillator cavity. Extending the length between the highly reflective mirror and the dye laser material beyond 254 mm did not improve the divergence of the oscillator cavity.

Table 3. Divergence and Length Between Highly Reflective Mirror and Dye Laser Material

Length between mirror and dye material, mm	Dye laser divergence, mrad
152	5
215	3
254	1
305	1

4.2.6. Mode Structure

For efficient frequency doubling into the UV region, it would be desirable for the solid-state dye laser to operate at the fundamental mode. To lase at the fundamental mode, the oscillator cavity mirrors were adjusted vertically and the beam profile of the dye laser beam was measured with the beam profile meter. The video output of the beam profile meter consisted of two scans over the field of odd and even pixel lines of the camera. The laser sensor integrates each field for 0.03 sec and combines two rows of pixel lines to form the intensity lines. Figure 37 shows the beam profile of the dye laser beam at an energy of 6 mJ using the PM 597 dye material (molar of 2×10^{-4}) at a thickness of 15 mm. The measurement was taken 35 cm away from the output coupler mirror of the oscillator cavity. The lines that form the circles of the profile represent the various intensities of the dye laser beam. The intensity profiles are 13.5, 36.8, 50, 60.7, 86.5, and 95 percent of the peak intensity of the dye laser beam starting from the largest circle to the smallest circle. A slight improvement occurred in the beam profile when the dye laser energy was increased to 9 mJ as shown in figure 38. The dye laser beam showed a near

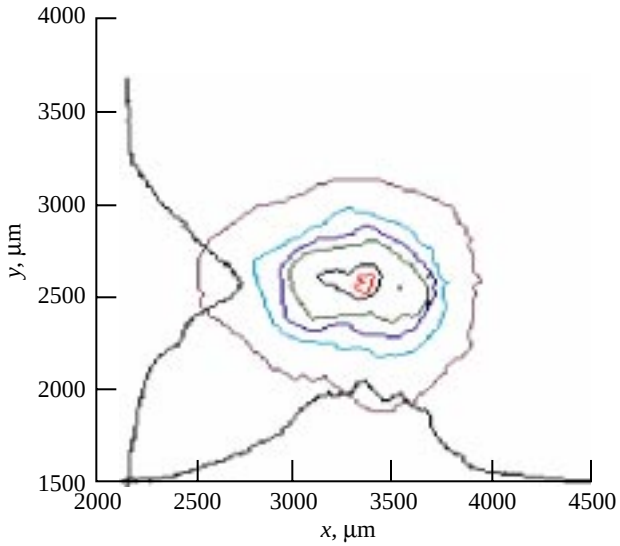

Figure 37. Beam profile of dye laser beam at energy of 6 mJ using PM 597 dye material (molar of 2×10^{-4}) at thickness of 15 mm.

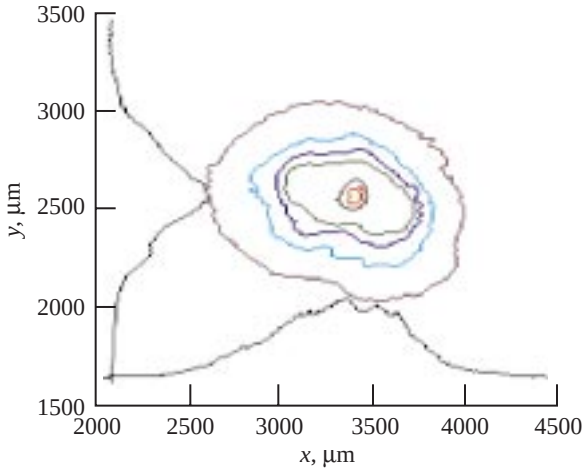

Figure 38. Beam profile of dye laser beam at energy of 9 mJ using PM 597 dye material (molar of 2×10^{-4}) at thickness of 15 mm.

Gaussian intensity profile in both the *x* and *y* dimensions when using the beam profile meter. The area of the highest intensity is located at the beam center. At a maximum dye laser energy of 11 mJ, the beam profile of the dye laser beam looked similar to the profile measured at a dye laser energy of 6 mJ as shown in figure 39. No significant changes were present in the profile at the maximum dye laser energy. The beam profiles shown in figures 38 and 39 show that the dye laser oscillator cavity is operating near the fundamental mode.

4.2.7. Second Harmonic Generation

Second harmonic generation was achieved by using the PM 597 dye laser material (molar of 2×10^{-4}) at a thickness of 15 mm by placing the BBO doubling crystal at the output of the dye laser oscillator cavity as shown in figure 16. To improve the efficiency of the doubling crystal, a half-wave plate and cylindrical convex lens with focal length of 100 mm were placed between the output coupler

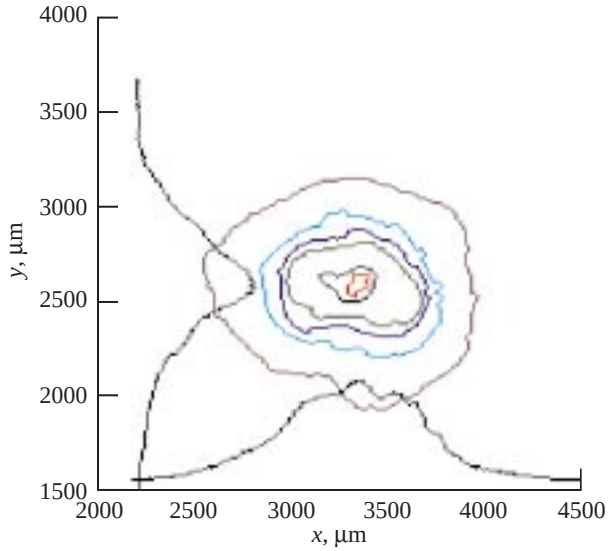

Figure 39. Beam profile of dye laser beam at energy of 11 mJ using PM 597 dye material (molar of 2×10^{-4}) at thickness of 15 mm.

and the input of the doubling crystal. The half-wave plate was used to rotate the polarization of the dye laser beam for maximum doubling efficiency, whereas the convex lens was used to increase the intensity of the dye laser beam in the BBO doubling crystal. The UV output energy from the doubling crystal was measured with the digital energy meter. The conversion efficiency was determined by taking the ratio of the UV energy at the output of the UV transmitting filter to the output energy of the dye laser.

The computer model defined in section 2 was used to predict the efficiency of the BBO doubling crystal with specific input parameters as measured in this investigation. The input parameters included the experimental results for line width (390 pm), beam divergence (1 mrad), dye laser energy (11 mJ), FWHM beam diameter (0.7 mm), crystal length (5 mm), pulse width (10 ns), and peak wavelengths of 578 or 600 nm. Figure 40 shows the theoretical calculation and experimental results of the conversion efficiency for the BBO doubling crystal at visible dye laser wavelengths of 578 or 600 nm. Only four data points were taken because of the limited range in dye laser energy that converted into the UV region. The PM 597 dye material was rotated to a new pump laser spot at each data point to make an accurate efficiency measurement. The experimental measurement was performed twice at each data point and the results are an average of the two measurements.

The highest conversion efficiency of the BBO doubling crystal was achieved experimentally at a maximum dye laser input energy of 11 mJ at a peak wavelength of 578 nm with the Nd:YAG 532 nm pump laser operating at 100 mJ. The computer model predicted the same conversion efficiency at both dye laser wavelengths of 578 and 600 nm. The digital energy meter measured 341 μJ of UV laser energy at the output of the UV transmitting filter. The UV laser energy increased to 378 μJ when taking into account the internal and external losses of the UV transmitting filter. A slight improvement in the conversion efficiency at 578 nm occurred because the intensity of the oscillator cavity at that wavelength is higher as shown by the laser tuning curve of figure 33. The computer model calculated a conversion efficiency of 5.9 percent when using the experimental results as the input parameters to the model. A factor of 2 difference occurred between the experimental and theoretical calculation of conversion efficiency at the maximum dye laser intensity. This difference in conversion efficiency may be due to the unconverted energy from the broad pedestal at the base of the spectral line width. The difference may also be due to the assumptions made by the computer model and the accuracy of the experimental measurements of divergence, line width, and UV output energy.

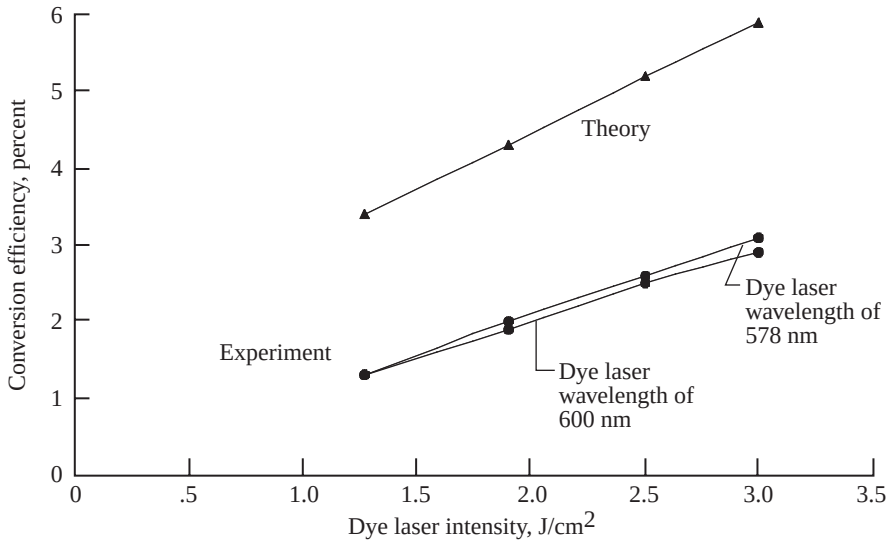

Figure 40. Experimental and theoretical calculations of conversion efficiency for BBO doubling crystal. Wavelengths for experimental curve of dye laser were 578 and 600 nm.

5. Concluding Remarks

In this report, a compact dye laser transmitter using a solid-state dye laser material was constructed and tested. Two types of solid-state dye laser materials were used to determine the most effective material for use in the dye laser transmitter. The conversion efficiency and lifetime of PM 580 doped in PMMA and PM 597 doped in MPMMA were tested in a broadband oscillator cavity configuration. The results of the test indicate that the PM 597 dye laser material has a higher slope efficiency at 79 percent and an improved resistance optical damage.

The efficiency of the PM 597 dye laser material was tested in a narrowband oscillator cavity configuration at different concentrations and thicknesses to determine the most efficient conversion from the pump laser wavelength of 532 nm to the dye laser wavelength of 578 nm. The lifetime, tunability, line width, and beam divergence of the oscillator cavity were measured with a molar of 2×10^{-4} of the PM 597 dye laser material with a thickness of 15 mm to determine the maximum conversion efficiency into the UV region with the BBO doubling crystal.

A computer model was used to compare the theoretical and experimental results of the conversion efficiency of the BBO doubling crystal. The results of the comparison between the computer model and the experimental results were fairly close. The doubling crystal had a low conversion efficiency due to the large beam divergence, large spectral line width, low dye laser intensity, and a low slope efficiency of 16 percent from the pump wavelength to the dye laser wavelength.

Improvements to the design of the oscillator cavity resulting in a smaller beam divergence and a narrower spectral line width should improve the conversion efficiency of the BBO doubling crystal. To improve the lifetime of the material, the dye laser material may be placed on a motorized rotation stage to decrease the damaging effects of the pump laser at one spot on the material. An oscillator-amplifier design should improve the conversion efficiency from the pump to the dye laser wavelength and improve the second harmonic conversion efficiency. Further scaling of this solid-state dye laser transmitter would be necessary for possible use in an ozone DIAL laser system.

References

1. Hinkley, E. D., ed.: *Laser Monitoring of the Atmosphere*. Springer-Verlag, 1976.

2. Killinger, D. K.; and Mooradian, Aram, eds.: *Optical and Laser Remote Sensing*. Springer-Verlag, 1983.

3. Adams, R. M.; Hamilton, S. A.; and McCarl, B. A.: An Assessment of the Economic Effects of Ozone on U.S. Agriculture. *J. Air Pollut. Control Assoc.*, vol. 35, 1985, pp. 938–943.

4. *Scientific Assessment of Ozone Depletion, 1994*. Global Ozone Res. & Monit. Proj. Rep. no. 37. World Meteorol. Organ., U.N. Environ. Programme, NOAA, and NASA, 1995.

5. Watson, Robert T.; Dixon, John A.; Hamburg, Steve P.; Janetos, Anthony C.; and Moss, Richard H.: *Protecting Our Planet—Securing Our Future: Linkages Among Global Environmental Issues and Human Needs*. U.N. Environ. Programme, NASA, and World Bank, 1998.

6. Tevini, Manfred, ed.: *UV-B Radiation and Ozone Depletion: Effects on Humans, Animals, Plants, Microorganisms, and Materials.* Lewis Publ., 1993.

7. Browell, E. V.: Differential Absorption Lidar Sensing of Ozone. *Proc. IEEE*, vol. 77, no. 3, 1989, pp. 419–432.

8. McPeters, Richard: *Total Ozone Mapping Spectrometer.* http://toms.gsfc.nasa.gov Accessed Mar. 28, 2001.

9. Killinger, Dennis; and Menyuk, Norman: Laser Remote Sensing of the Atmosphere. *Science*, vol. 235, 1987, p. 37.

10. Smullin, L. D.; and Fiocco, G.: *Nature*, vol. 194, 1962, p. 1267.

11. Schotland, R. M.: Some Observations of the Vertical Profile of Water Vapor by Means of a Laser Optical Radar. *Proceedings of the Fourth Symposium on Remote Sensing of the Environment*, ERIM, 1966, pp. 273–283.

12. Browell, E. V.; Carter, A. F.; Shipley, S. T.; Allen, R. J.; Butler, C. F.; Mayo, M. N.; Siviter, J. H., Jr.; and Hall, W. M.: The NASA Multipurpose Airborne DIAL System and Measurements of Ozone and Aerosol Profiles. *Appl. Opt.*, vol. 22, no. 4, Feb. 1983, pp. 522–534.

13. Browell, E. V.; Ismail, S.; and Grant, W. B.: Differential Absorption Lidar (DIAL) Measurements From Air and Space. *Appl. Phys. B*, vol. 67, no. 4, 1998, pp. 399–410.

14. Kopylova, Tat'yana N.; Reznichenko, A. V.; Mayer, Georgy V.; Samsonova, Lyubov'g; Svetlichny, V. A.; Kuznetsova, Rimma T.; Sukhanov, V. B.; and Telminov, E. N.: Blue-Green Laser Radiation From Dyes in Matrix. *Proc. SPIE*, Vol. 3403, 1998, pp. 182–185.

15. Stuke, M.: Dye Lasers, 25 Years. *Topics Appl. Phys.*, vol. 70, 1992, p. 19.

16. Allik, Toomas H.; Chandra, Suresh; Utano, Richard; Robinson, Timothy R.; and Boyer, Joseph H.: *Improved Longevities and Novel Wavelength Generation From a Solid-State Dye Laser*. Korry Electron. Co., 2000. http://www.korry.com/technical.html Accessed May 9, 2001.

17. Soffer, B. H.; and Farland, B. B.: Continuously Tunable, Narrow-Band Organic Dye Lasers. *Appl. Phys. Lett.*, vol. 10, 1967, pp. 266–267.

18. Allik, Toomas H.; Hermes, Robert E.; Sathyamoorthi, Govindarao; and Boyer, Joseph H.: Spectroscopy and Laser Performance of New BF_2-Complex Dyes in Solution. *Proc. SPIE*, Vol. 2115, 1994, pp. 240–248.

19. Shah, Mayur; Thangaraj, Kannappan; Mou-Ling, Soong; Wolford, Lionel T.; Boyer, Joseph H.; Politxer, Leva R.; and Pavlopoulos, Theodore: Pyrromethene-BF_2 Complexes as Laser Dyes. *Heteroatom Chem.*, vol. 1, no. 5, Oct. 1990, pp. 389–400.

20. Pavlopoulos, T. G.; Shah, M.; and Boyer, J. H.: Efficient Laser Action From 1,3,5,7,8-Pentamethylpyrromethene-BF_2 Complex and Its Disodium 1,6-Disulfonate Derivative. *Opt. Comm.*, vol. 70, no. 5, 1989, p. 425.

21. Dyumaev, K. M.; Manenkov, A. A.; Maslyukov, A. P.; Matyushin, G. A.; Nechitailo, V. S.; and Prokhorov, A. M.: Dyes in Modified Polymers: Problems of Photostability and Conversion Efficiency at High Intensities. *J. Opt. Soc. America B*, vol. 9, no. 1, Jan. 1992, pp. 143–154.

22. Jones, Alton L., Jr.: A Compact Ozone Differential Absorption Lidar (DIAL) Transmitter Using a Solid-State Dye Polyer. M.S. Thesis, Old Dominion Univ., Dec. 2000.

23. Schoulepnikoff, L.; Van Den Bergh, H.; Calpini, B., and Mitev, V.: Tropospheric Air Pollution Monitoring, LIDAR. *Encyclopedia of Environmental Analysis and Remediation*, Robert A. Meyers, ed., John Wiley & Sons, Inc., 1998, pp. 4873–4909.

24. Byer, R.: Review—Remote Air Pollution Measurement. *Opt. & Quantum Electron.*, vol. 7, no. 3, May 1975, pp. 147–177.

25. Milonni, Peter W.; and Eberly, Joseph H.: *Lasers*. John Wiley & Sons, Inc., 1988, p. 635.

26. Agrawal, Govind P.; and Boyd, Robert W., ed.: *Contemporary Nonlinear Optics*. Academic Press, 1992, p. 4.

27. Koechner, Walter: *Solid-State Laser Engineering*, 2nd ed. Springer-Verlag, 1988, p. 478.

28. Sutherland, Richard Lee.: *Handbook of Nonlinear Optics*. Marcel Dekker, Inc., 1996, pp. 36–49.

29. Graham-Smith, Francis; and Thomson, John Hunter: *Optics*. John Wiley & Sons, Inc., 1988, p. 266.

30. Dmitriev, Valentin Georgievch; Gurzadyan, Gagik G.; and Nikogosyan, D. N.: *Handbook of Nonlinear Optical Crystals*. Springer-Verlag, 1991, p. 5.

31. Hagen, W. F.; and Magnante, P. C.: Efficient Second-Harmonic Generation With Diffraction-Limited and High-Spectral-Radianced-Glass Lasers. *J. Appl. Phys*., vol. 40, 1969, p. 219.

32. Allik, Toomas H.; Chandra, Suresh; Robinson, Timothy R.; Hutchinson, J. Andrew; Sathyamoorthi, Govindarao; and Boyer, Joseph H.: Laser Performance and Material Properties of a High Temperature Plastic Doped With Pyrromethene-BF_2 Dyes. *Proceedings of the Materials Research Society Symposium*, vol. 329, 1994, pp. 291–296.

33. Chandra, S.; Allik, T.; and Hutchinson, J.: Nonconfocal Unstable Resonator for Solid-State Dye Lasers Based on a Gradient-Reflectivity Mirror. *Opt. Lett.*, vol. 20, 1995, pp. 2387–2389.

34. Bowers, Mark; Allik, Toomas; Chandra, Suresh; and Hutchinson, J. Andrew: Optimized Graded-Reflectivity Unstable Resonator for Laser Pumped Solid-State Dye Laser. *Proceedings of the International Conference on Lasers '95*, 1995, pp. 366–372.

35. Nair, L. G.; and Dasgupta, K.: Amplified Spontaneous Emission in Narrow-Band Pulsed Dye Laser Oscillators: Theory and Experiment. *IEEE J. Quantum Electron*., vol. QE-21, no. 11, 1985, pp. 1782–1794.

REPORT DOCUMENTATION PAGE

Form Approved
OMB No. 0704-0188

1. AGENCY USE ONLY *(Leave blank)*	2. REPORT DATE	3. REPORT TYPE AND DATES COVERED
	July 2001	Technical Memorandum

4. TITLE AND SUBTITLE
Compact Ozone Differential Absorption Lidar (DIAL) Transmitter Using Solid-State Dye Polymers

5. FUNDING NUMBERS
WU 622-63-13-70

6. AUTHOR(S)
Alton L. Jones, Jr., Russell J. DeYoung, and Hani Elsayid-Ele

7. PERFORMING ORGANIZATION NAME(S) AND ADDRESS(ES)
NASA Langley Research Center
Hampton, VA 23681-2199

8. PERFORMING ORGANIZATION REPORT NUMBER
L-18062

9. SPONSORING/MONITORING AGENCY NAME(S) AND ADDRESS(ES)
National Aeronautics and Space Administration
Washington, DC 20546-0001

10. SPONSORING/MONITORING AGENCY REPORT NUMBER
NASA/TM-2001-211028

11. SUPPLEMENTARY NOTES
Jones and Elsayid-Ele: Old Dominion University, Norfolk, VA; DeYoung: Langley Research Center, Hampton, VA.

12a. DISTRIBUTION/AVAILABILITY STATEMENT
Unclassified–Unlimited
Subject Category 36 Distribution: Standard
Availability: NASA CASI (301) 621-0390

12b. DISTRIBUTION CODE

13. ABSTRACT ***(Maximum 200 words)***

A new potential DIAL laser transmitter is described that uses solid-state dye laser materials to make a simpler, more compact, lower mass laser system. Two solid-state dye laser materials were tested to evaluate their performance in a laser oscillator cavity end pumped by a pulsed Nd:YAG laser at 532 nm. The polymer host polymethylmethacrylate was injected with a pyrromethene laser dye, PM 580, or PM 597. A narrowband laser oscillator cavity was constructed to produce visible wavelengths of 578 and 600 nm which were frequency doubled into the UV region (289 or 300 nm) by using a BBO crystal, resulting in a maximum energy of 11 mJ at a wavelength of 578 nm when pumped by the Nd:YAG laser at an energy of 100 mJ (532 nm). A maximum output energy of 378 μJ was achieved in the UV region at a wavelength of 289 nm but lasted only 2000 laser shots at a repetition rate of 10 Hz. The results are promising and show that a solid-state dye laser based ozone DIAL system is possible with improvements in the design of the laser transmitter.

14. SUBJECT TERMS	15. NUMBER OF PAGES
Dye laser; Solid-state dye; Ozone laser transmitter; DIAL	49
	16. PRICE CODE

17. SECURITY CLASSIFICATION OF REPORT	18. SECURITY CLASSIFICATION OF THIS PAGE	19. SECURITY CLASSIFICATION OF ABSTRACT	20. LIMITATION OF ABSTRACT
Unclassified	Unclassified	Unclassified	UL